Clearing the Air: A Chemical Approach to Understanding Secondary Organic Aerosol Formation From Volatile Chemical Products

Thesis by
Reina S. Buenconsejo

In Partial Fulfillment of the Requirements for the
Degree of
PhD in Chemistry

CALIFORNIA INSTITUTE OF TECHNOLOGY
Pasadena, California

2024
Defended April 12, 2024

Reina S. Buenconsejo
ORCID: 0000-0002-0162-905X

ACKNOWLEDGEMENTS

Thank you to everyone who helped me along this journey of discovery and growth—both as a scientist and as a person. Thank you to my advisors, Paul Wennberg and John Seinfeld. Thank you both for the innumerable contributions you've made to our field which have made it possible to study the contents of this thesis. Thank you, Paul, for sharing your love of chemistry, and for all of your advice over the years. Thank you, John, for your unending support.

Thank you to my thesis committee members Rick Flagan and Mitchio Okumura. Rick, thank you for your always being a great committee chair. Thank you, Mitchio, for your kindness, support, and thoughtful questions and discussion.

Fred Grieman, thank you for all of your mentorship over the years. Thank you Anne Yu for all of your support and for teaching me to advocate for myself as a professional.

Thank you to my labmates and friends at Caltech. Sophia Charan, you taught me everything I know in the Seinfeld lab. You gave me a sense of direction and you inspire a genuineness and kindness in us all. Thank you Lu Xu for your mentorship and patience. Yuanlong Huang, you've helped me in more ways than I can count. I'm in awe of your dedication and generosity. Thank you to Chris Kenseth for teaching me how to use the UPLC-MS and for always being around to talk chemistry. Thank you to Chris, Ben Schulze, and Ryan Ward for being the guardians of the AMS. Ben, your positivity is infectious and your work ethic is something I look up to. Ryan, thank you for being a greater Spanish Colloquium treasurer. Elyse, thank you for your friendship and shared love of tea. Thank you to Sara Murphy, without whom I would not have survived either of our field campaigns—you are both a great scientist and friend. Thank you Harrison Parker for being such a considerate friend and colleague.Thank you, also, for introducing me to your wife, Jackie Lopez Parker. Jackie—thank you for your friendship.

Thank you to my mentees, Maria Yu and and Haroula Baliaka, for trusting me to teach you about our lab and our instrumentation. Haroula, thank you, also, for eventually becoming my mentor and confidante. I'm not sure what I would have done these last two years without you.

Thank you to Dien Wu and Josh Laughner for being great office mates. You inspire me to try new coding languages and to be a better data steward. Thank you to

Danielle Draper, Ariana Tribby, Kat Ball, John Crounse, Coleen Rohl, and Nathan Dalleska. Thank you to all of the past Seinfeld and Wennberg Lab members, especially those who built and/or cared for the environmental chambers and the GC-CIMS. And thank you to our honorary atmospheric chemist, Lily Dove, for your friendship and advocacy.

Thank you to Katie Page, Marta Gonzalvo, Mark Zhang, and all of my peers in CCE: you make my life and the scientific community better. Thank you to the Dolores Mission community who also fight for a better community.

Thank you Alison Ross, Nora Oshima, and Bronagh Glasser for everything you do to make the Linde Center and CCE run smoothly. Thank you to the library staff, especially Donna Wrublewski and Kathy Johnson.

Thank you to my STPI and Sandia mentors who helped shaped my career path and whom I find inspiration in!

Thank you to my friends and family for your years of love and support: Andrea, Meghan, Reid, the Amigas (Regina, Megan, Yung, and Chloe). To my 19 aunts and uncles, 18 first cousins, and 16 second cousins, thank you for being my village. Thank you to my in-laws, especially Kevin, Maureen, and JP, for becoming a part of my extended family.

To my mom and dad, thank you for everything. Dad, thank you for being my first science mentor (first grade science fair), and for all of the life lessons since then. Mom, you are my inspiration. I hope I can grow up to be like you. I love you both.

To my husband, Sean, thank you for being my person. My best discovery yet has been finding you. I love you.

ABSTRACT

Understanding sources of air pollution is critically important as ~ 7 million premature deaths are associated with poor air quality (World Health Organization, 2024). A key component of urban air quality is secondary organic aerosol (SOA), a type of particulate matter that contributes smog. SOA is formed via the reactive oxidation of volatile organic chemicals (VOCs), gas-phase compounds often emitted from anthropogenic sources. Historically, SOA formation and VOC emissions have been driven by on-road mobile sources. In recent years, however, other sources, such as consumer and industrial solvents—so called volatile chemical products (VCPs)—have become increasingly more important. SOA also impacts climate change, as particulate matter affects global radiative forcing.

Characterizing the chemistry and SOA formation from VCPs can elucidate our understanding of modern urban air pollution, particularly as we try to uncover recent stagnation in air quality. Because VCPs are comprised of hundreds of individual chemical compounds, it is exceedingly difficult to study and characterize each one individually. By contrast, understanding these compounds through a chemistry lens can help to make broader generalizations about larger classes of compounds.

This dissertation looks at the chemistry leading to SOA formation from several chemicals that make up VCPs. Specifically, this work looks at benzyl alcohol and ethoxyethanol. These compounds are used in personal care products, cleaning products, architectural coatings and adhesives. Prior to this work, both were considered to have modest SOA yields at ambient atmospheric conditions ($< 10\%$).

Understanding the reactivity of these compounds can help us understand more broadly the chemistry and SOA potential of other chemicals in VCPs that have similar chemical structures. Studying the chemistry and SOA formation of VCPs under a variety of [NO] and RO_2 bimolecular lifetime conditions is also imperative as ambient urban environments continue to evolve.

PUBLISHED CONTENT AND CONTRIBUTIONS

Buenconsejo, Reina, Baliaka, Haroula, Wennberg, Paul, and Seinfeld, John (2024). "Formation of Secondary Organic Aerosol from Glycol Ethers". In: *ACS ES&T Air, In Prep*.
RSB conceptualized the study, performed data collection and analysis, interpreted the results, and wrote the manuscript.

Buenconsejo, Reina S., Sophia M. Charan, John H. Seinfeld, and Paul O. Wennberg (Nov. 8, 2023). "Quantifying primary oxidation products in the OH-initiated reaction of benzyl alcohol". In: DOI: 10.5194/egusphere-2023-2483. URL: https://egusphere.copernicus.org/preprints/2023/egusphere-2023-2483/.
RSB conceptualized the study, performed data collection and analysis, interpreted the results, and wrote the manuscript.

Yu, Hongmin, Kristian H. Møller, **Buenconsejo, Reina** S., John D. Crounse, Henrik G. Kjaergaard, and Paul O. Wennberg (Nov. 7, 2023). "Atmospheric Photo-Oxidation of 2-Ethoxyethanol: Autoxidation Chemistry of Glycol Ethers". In: *The Journal of Physical Chemistry A*, acs.jpca.3c04456. ISSN: 1089-5639, 1520-5215. DOI: 10.1021/acs.jpca.3c04456. URL: https://pubs.acs.org/doi/10.1021/acs.jpca.3c04456.
RSB assisted with laboratory experiments, discussions about science and data analysis, and edited the manuscript

Charan, Sophia M., **Buenconsejo, Reina S.**, and John H. Seinfeld (Nov. 10, 2020). "Secondary organic aerosol yields from the oxidation of benzyl alcohol". In: *Atmospheric Chemistry and Physics* 20.21, pp. 13167–13190. ISSN: 1680-7324. DOI: 10.5194/acp-20-13167-2020. URL: https://acp.copernicus.org/articles/20/13167/2020/.
RSB assisted with chamber experiments, collected UPLC-MS data, and participated in the writing of the manuscript.

TABLE OF CONTENTS

LIST OF ILLUSTRATIONS

LIST OF TABLES

NOMENCLATURE

°C. Degrees centigrade.

HO_2. Hydroperoxyl radical.

NO_2. Nitric dioxide.

NO_x. Nitrogen oxides which includes NO and NO_2.

PM_{10}. Particulate matter 10 μm in size or smaller.

$PM_{2.5}$. Particulate matter 2.5 μm in size or smaller.

RO_2. Peroxy radical.

cm. Centimeter.

g. Gram.

h. Hours.

K. Kelvin.

L. Liter.

Lpm. Liters per minute.

m. Meter.

min. Minutes.

molec. Molecule.

nm. Nanometer.

NO. Nitric oxide.

OH. Hydroxyl radical.

PM. Particulate matter.

ppb. Parts per billion.

ppm. Parts per million.

ppt. Parts per trillion.

RO. Alkoxy radical.

s. Second.

SOA. Secondary organic aerosol.

VCP. Volatile chemical products.

VOC. Volatile organic compound.

Chapter 1

INTRODUCTION

1.1 Background and Motivation

The World Health Organization (WHO) estimates that 99% of the global population are exposed to high levels of air pollution (World Health Organization, 2024). An estimated 7 million premature deaths are attributed to air pollution annually (World Health Organization, 2024). Indoor and outdoor air quality can be driven by a number of sources including vehicular emissions, industrial processes, stationary fuel combustion, cooking, landfills, among others. These sources emit a number pollutants such as volatile organic chemicals (VOCs), particulate matter (PM)—both fine PM under $2.5\mu m$ ($PM_{2.5}$) and coarse PM under $10\mu m$ (PM_{10}), ozone (O_3), and nitrogen oxides (NO_x) such as nitrogen oxide (NO) and nitrogen dioxide (NO_2). Tropospheric O_3, PM, and NO_x are key components of smog. While some VOCs and NO_x can be acutely toxic to breathe, they can also go on to react to form additional ozone and PM. Understanding the chemistry and formation of these components of air pollution is key to understanding ways to improve overall air quality.

As one of the most polluted regions in the United States, the South Coast Air Basin (SoCAB), which includes Orange County, two-thirds of Los Angeles County, and the western portions of Riverside and San Bernardino Counties, has faced challenges in meeting national air quality standards (Riverside-Corona Resource Conservation District, 2024). Historically, improvements to SoCAB have been driven by reductions in vehicular emissions (Fujita et al., 2013). Since the implementation of the catalytic converter, $PM_{2.5}$ concentrations in the LA area have decreased by 57% (Air Quality Life Index, 2024).

However, over the past 10 years in SoCAB, improvements in certain air pollution metrics have slowed despite continued reductions in vehicular emissions. For example, NO_2, which is closely correlated to mobile sources, has continually decreased over the past several decades. However, ozone and $PM_{2.5}$ have remained nearly constant over the past 10 years (Figure 1.1). Other regions across the U.S. have also struggled to meet air quality standards despite significant reductions in vehicular emissions, and therefore NO_2 (NASA, 2023). Over 92% of the U.S. population lives

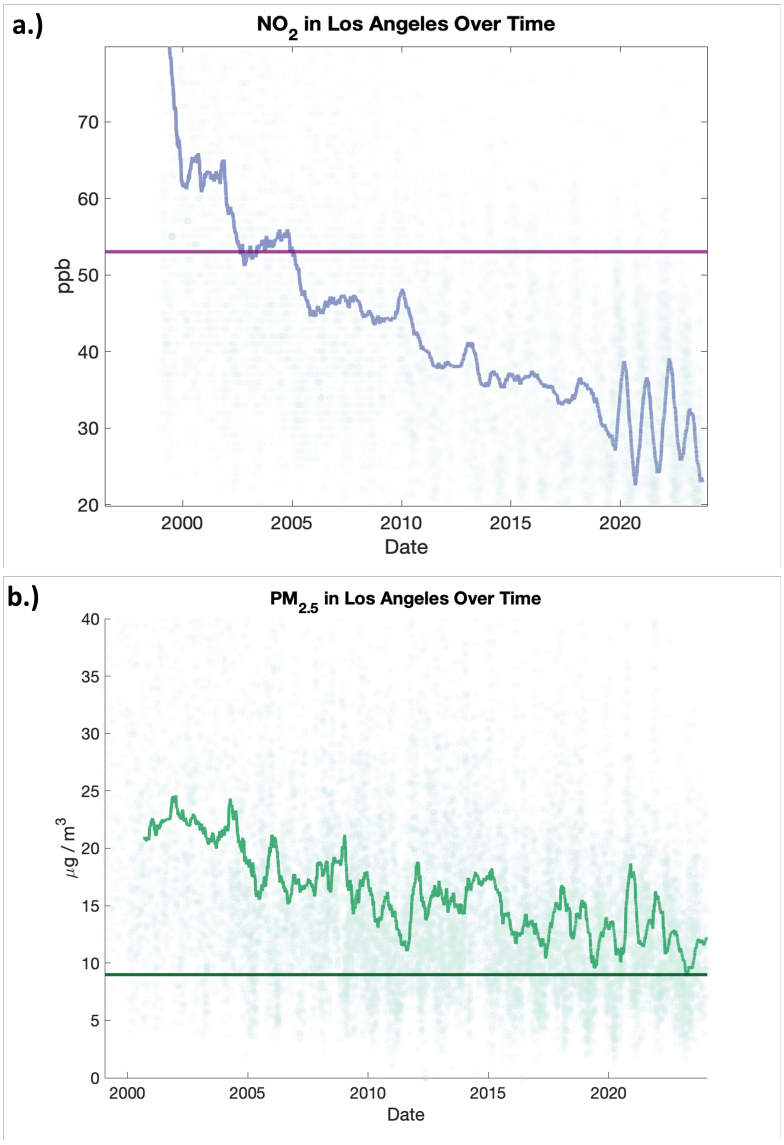

Figure 1.1: NO_2 has decreased over time due to regulations in mobile source emissions (Panel (a)). $PM_{2.5}$ has decreased less over time and has flat-lined in the past $\sim$ 10 years (Panel (b)). Data are from the North Main Street EPA monitoring station in LA.

in areas that do not meet the WHO standard for annual average $PM_{2.5}$ standard of 5 $\mu g\, m^{-3}$ (Air Quality Life Index, 2024).

To understand why U.S. urban areas continue to experience persistently poor air quality, it is important to consider other sources of air pollutants beyond mobile emissions. Modeling and field work have identified volatile chemical products (VCPs) as increasingly important sources of pollution and pollution precursors (McDonald et al., 2018; Pennington et al., 2021; Coggon et al., 2021; Seltzer et al.,

2021). VCPs include industrial and consumer products such as cleaning products, personal care products, pesticides, and paints. In terms of mass used per year, VCPs have a relatively small usage compared to gasoline and diesel fuels (McDonald et al., 2018). Despite this, VCPs make up a larger apportionment of VOC emissions. For example, McDonald et al. (2018) estimated that while VCPs make up 4% of total hydrocarbon usage (calculated as teragrams used per year), they make up 38% of all VOC emissions. It is also estimated that after the VOCs are emitted from VCPs, their potential reactivity with OH, the primary atmospheric daytime oxidant, is greater than VOCs emitted from gasoline and diesel fuel sources (McDonald et al., 2018). When these VOCs oxidize, they can form lower volatility products that eventually partition into secondary organic aerosol (SOA), an important type of PM that contributes significantly to total $PM_{2.5}$. McDonald et al. (2018) estimates that the VOC reactivity and potential to form SOA for VCPs is 46% and 42%, respectively. Understanding VOC emissions and the reactivity of VOCs can thus elucidate SOA formation.

Models that include VCP emissions and chemistry have shown improvements compared to observed ozone and $PM_{2.5}$ versus when VCPs are excluded (Pennington et al., 2021). Yet, at present, models are still unable to fully account for observations. This suggests that our understanding of VOC reactivity from VCPs may be incomplete. Thus, understanding the reactivity and characterizing the SOA yields (the mass ratio of VOC reacted to form SOA) from VCPs is crucial to understanding current ozone and $PM_{2.5}$ trends in urban areas like SoCAB.

Studying VCP reactivity over a variety of conditions is also critically important to understanding air quality. This is particularly true in urban areas where NO_x conditions have changed over time. Considerable work has been done in the past to understand the reaction of VOCs in the presence of NO which forms NO_2 and eventually ozone. However, as NO continues to decline in urban centers, such as SoCAB, the atmospheric chemistry shifts towards a so-called NO_x-limited regime (Kroll et al., 2020). In lower NO_x environments, autoxidation can occur. Autoxidation involves intermolecular H-shifts within a peroxy radical intermediate (Figure 1.2) (Crounse et al., 2013). This reaction has shown to be important in a number of atmospherically relevant compounds though remains unaccounted for several VCP systems. Thus, this thesis will describe chemistry under a variety of different [NO] conditions.

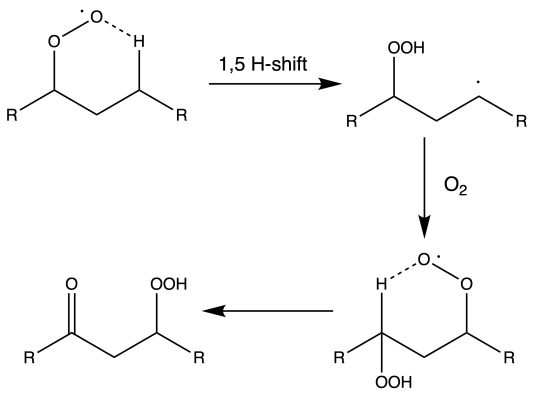

Figure 1.2: Example of unimolecular peroxy radical H-shift that occurs in the autoxidation scheme.

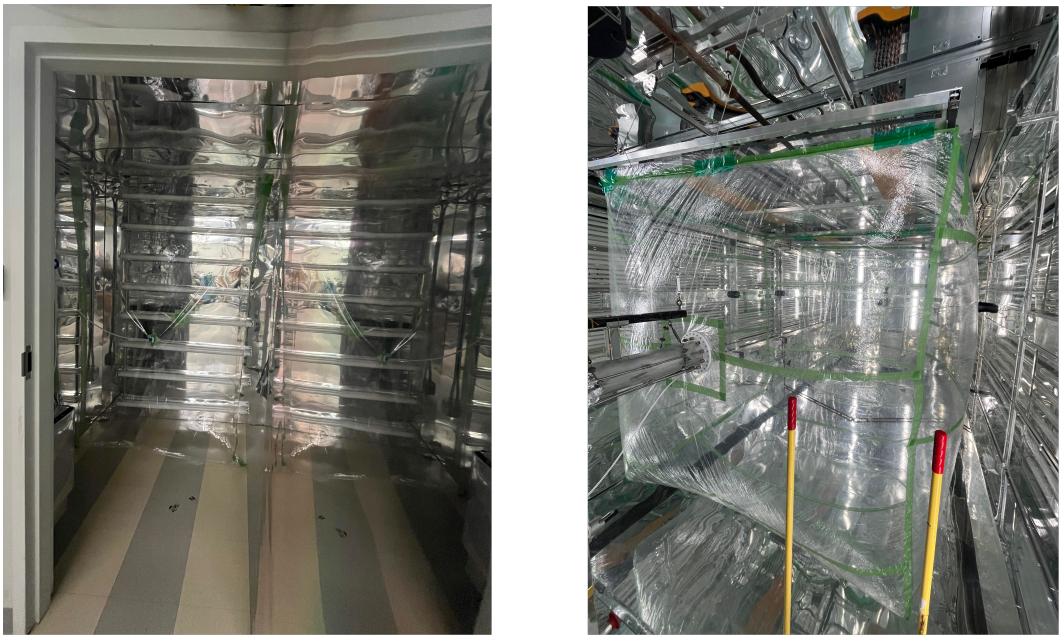

Figure 1.3: This thesis describes work conducted in two environmental chambers. Left: A $\sim$ 0.1 m^3 environmental chamber used to study gas-phase chemistry. Right: Two $\sim$ 19 m^3 environmental smog chambers used to study SOA formation, composition, and yields.

To study the chemistry and SOA formation of VCPs in this thesis, a variety of laboratory tools were employed. This thesis presents work conducted in two batch mode reactors: the Caltech Environmental Smog Chamber and a photolytic environmental chamber (Figure 1.3). Experiments in these environmental chambers help simulate the reactivity of VCP emissions in the real atmosphere. This thesis explores the daytime chemistry of and SOA formation from two VCP chemicals: benzyl alcohol and ethoxyethanol.

1.2 Organization of Thesis

This thesis explores the atmospheric chemistry of VCPs as an increasingly important VOC-emission source. The VCPs used for this thesis were studied under a variety of atmospheric conditions, including in NO_x limited regimes (Chapter 4). By understanding the chemistry of various chemicals found in VCPs (Chapters 2 and 4), this thesis explores the SOA formation and quantifies the SOA yields from VCPs (Chapters 3 and 4).

Chapter 2 discusses the chemistry of benzyl alcohol, a solvent widely used in consumer products and as an industrial solvent. This chapter describes a general chemical mechanism of benzyl alcohol oxidation under low-NO and high-NO conditions. Using gas chromatography in tandem with mass spectrometry, I identified a number of oxidation products formed from the reaction of benzyl alcohol and quantified branching ratios of the primary products. In this chapter, I compare the oxidative chemistry of benzyl alcohol to other aromatic compounds. Similar to other aromatics, benzyl alcohol primarily reacts via one of two chemical pathways: 1.) addition or 2.) abstraction. Chapter 2 also describes observed C6 compounds that form and may also form SOA.

The chemistry of benzyl alcohol can help inform how products may eventually contribute to SOA formation. Chapter 3 reports on SOA studies conducted to quantify benzyl alcohol SOA yields and understand how different chemical pathways contribute to SOA formation. Work in this chapter describes SOA experiments conducted with the primary oxidation products of benzyl alcohol: hydroxybenzyl alcohol and benzaldehyde. Both compounds have considerable yields ranging from ~ 1 to ~ 0.3, respectively, suggesting that benzyl alcohol should also have a significant SOA yield. Indeed, Chapter 3 also details SOA yield studies of benzyl alcohol directly which indicates that under certain conditions, the yield approaches unity.

Chapter 4 looks at ethoxyethanol as a model for a class of compounds called glycol ethers. These chemical compounds are pervasive in cleaning products and also found in soaps, dyes, inks, paints, and cosmetics. The work presented in Chapter 4 considers the chemistry of ethoxyethanol under a variety of peroxy radical (RO_2) bimolecular lifetimes. By adjusting the bimolecular lifetime, the glycol ether will react via different chemical pathways to different extents. With sufficiently high bimolecular lifetimes, ethoxyethanol reacts via autoxidation, a unimolecular reaction involving internal hydrogen shifts. Chapter 4 presents SOA yield data suggesting the autoxidation of glycol ethers is an efficient way to produce SOA.

Appendices A and B each present selected published papers about VCPs on which I am a co-author. Appendix A includes a paper that expands on the work from Chapter 4. This paper provides greater detail to the oxidative chemical mechanism of ethoxyethanol under different RO_2 lifetimes. Appendix B includes work on a different VCP, decamethylcyclopentasiloxane (D5 siloxane). This paper primarily looks at the SOA yield of D5 siloxane under a range of OH mixing ratios.

References

Air Quality Life Index (2024). *United States: Clean Air Act (1970)*. URL: https://aqli.epic.uchicago.edu/policy-impacts/united-states-clean-air-act/#:~:text=With%20less%20pollution%20in%20the,average%20Angeleno%20by%201.5%20years..

Coggon, Matthew M., Georgios I. Gkatzelis, Brian C. McDonald, Jessica B. Gilman, Rebecca H. Schwantes, Nader Abuhassan, Kenneth C. Aikin, Mark F. Arend, Timothy A. Berkoff, Steven S. Brown, Teresa L. Campos, Russell R. Dickerson, Guillaume Gronoff, James F. Hurley, Gabriel Isaacman-VanWertz, Abigail R. Koss, Meng Li, Stuart A. McKeen, Fred Moshary, Jeff Peischl, Veronika Pospisilova, Xinrong Ren, Anna Wilson, Yonghua Wu, Michael Trainer, and Carsten Warneke (Aug. 2021). "Volatile chemical product emissions enhance ozone and modulate urban chemistry". en. In: *Proceedings of the National Academy of Sciences* 118.32, e2026653118. ISSN: 0027-8424, 1091-6490. DOI: 10.1073/pnas.2026653118. URL: https://pnas.org/doi/full/10.1073/pnas.2026653118 (visited on 05/16/2022).

Crounse, John D., Lasse B. Nielsen, Solvejg Jørgensen, Henrik G. Kjaergaard, and Paul O. Wennberg (Oct. 2013). "Autoxidation of organic compounds in the atmosphere". en. In: *The Journal of Physical Chemistry Letters* 4.20, pp. 3513–3520. ISSN: 1948-7185, 1948-7185. DOI: 10.1021/jz4019207. URL: https://pubs.acs.org/doi/10.1021/jz4019207 (visited on 10/28/2021).

Fujita, Eric M., David E. Campbell, William R. Stockwell, and Douglas R. Lawson (Jan. 2013). "Past and future ozone trends in California's South Coast Air Basin: Reconciliation of ambient measurements with past and projected emission inventories". en. In: *Journal of the Air & Waste Management Association* 63.1, pp. 54–69. ISSN: 1096-2247, 2162-2906. DOI: 10.1080/10962247.2012.735211. URL: https://www.tandfonline.com/doi/full/10.1080/10962247.2012.735211 (visited on 02/05/2024).

Kroll, Jesse H., Colette L. Heald, Christopher D. Cappa, Delphine K. Farmer, Juliane L. Fry, Jennifer G. Murphy, and Allison L. Steiner (Sept. 2020). "The complex chemical effects of COVID-19 shutdowns on air quality". en. In: *Nature Chemistry* 12.9, pp. 777–779. ISSN: 1755-4330, 1755-4349. DOI: 10.1038/s41557-020-0535-z. URL: http://www.nature.com/articles/s41557-020-0535-z (visited on 09/01/2020).

McDonald, Brian C., Joost A. de Gouw, Jessica B. Gilman, Shantanu H. Jathar, Ali Akherati, Christopher D. Cappa, Jose L. Jimenez, Julia Lee-Taylor, Patrick L. Hayes, Stuart A. McKeen, Yu Yan Cui, Si-Wan Kim, Drew R. Gentner, Gabriel Isaacman-VanWertz, Allen H. Goldstein, Robert A. Harley, Gregory J. Frost, James M. Roberts, Thomas B. Ryerson, and Michael Trainer (Feb. 2018). "Volatile chemical products emerging as largest petrochemical source of urban organic emissions". en. In: *Science* 359.6377, pp. 760–764. ISSN: 0036-8075, 1095-9203.

DOI: 10.1126/science.aaq0524. URL: http://www.sciencemag.org/lookup/doi/10.1126/science.aaq0524 (visited on 10/12/2018).

NASA (May 2023). *Two Decades of Changes in Nitrogen Dioxide and Fine Particulate Pollution in the U.S.* URL: https://svs.gsfc.nasa.gov/5104/.

Pennington, Elyse A., Karl M. Seltzer, Benjamin N. Murphy, Momei Qin, John H. Seinfeld, and Havala O. T. Pye (Dec. 2021). "Modeling secondary organic aerosol formation from volatile chemical products". en. In: *Atmospheric Chemistry and Physics* 21.24, pp. 18247–18261. ISSN: 1680-7324. DOI: 10.5194/acp-21-18247-2021. URL: https://acp.copernicus.org/articles/21/18247/2021/ (visited on 05/19/2022).

Riverside-Corona Resource Conservation District (2024). *South Coast Air Quality Management District (SCAQMD)*. URL: https://www.rcrcd.org/south-coast-air-quality-management-district-scaqmd.

Seltzer, Karl M., Elyse Pennington, Venkatesh Rao, Benjamin N. Murphy, Madeleine Strum, Kristin K. Isaacs, and Havala O. T. Pye (Mar. 2021). "Reactive organic carbon emissions from volatile chemical products". en. In: *Atmospheric Chemistry and Physics* 21.6, pp. 5079–5100. ISSN: 1680-7324. DOI: 10.5194/acp-21-5079-2021. URL: https://acp.copernicus.org/articles/21/5079/2021/ (visited on 11/29/2022).

World Health Organization (2024). *Air Pollution*. URL: https://www.who.int/health-topics/air-pollution#tab=tab_2.

Chapter 2

OXIDATIVE CHEMISTRY OF BENZYL ALCOHOL

Buenconsejo, Reina S., Sophia M. Charan, John H. Seinfeld, and Paul O. Wennberg (Nov. 8, 2023). "Quantifying primary oxidation products in the OH-initiated reaction of benzyl alcohol". In: DOI: 10.5194/egusphere-2023-2483. URL: https://egusphere.copernicus.org/preprints/2023/egusphere-2023-2483/.

Abstract

Benzyl alcohol is a compound found in many volatile chemical products (VCPs), and is widely used in personal care products and as an industrial solvent. While past work has empirically identified oxidation products, we do not understand explicit branching fractions for first-generation benzyl alcohol oxidation products, particularly over a range of [NO] conditions. Using gas chromatography (GC) in tandem with chemical ionization mass spectrometry (CIMS) and gas chromatography with a flame ionization dectector (GC-FID), we measure the branching ratios of major oxidation products, namely hydroxybenzyl alcohol (HBA) and benzaldehyde. Later-generation oxidation products from both HBA and benzaldehyde pathways are also observed. We find the H-abstraction route leading to benzaldehyde formation unaffected by [NO], with a branching fraction of $\sim$ 21%. The OH addition route which leads to HBA formation also does not appear to vary with [NO]. We report a branching fraction for HBA of $\sim$ 34%. We also find that HBA has a high secondary organic aerosol (SOA) yield and, therefore, likely contributes to the high SOA yield of benzyl alcohol; under some conditions the yield can approach unity. Insights from the present study can help elucidate the chemistry of other atmospherically-relevant aromatic compounds, especially those found in VCPs.

2.1 Introduction

Recent work indicates the growing importance of volatile chemical products (VCPs) in driving air pollution chemistry, particularly as regulations decline the contribution of vehicular-based emissions (McDonald et al., 2018; Coggon et al., 2021). VCPs play an important role in air quality because of their high potential to form secondary organic aerosol (SOA); an analysis of VCPs in the Los Angeles Air Basin

indicates that VCPs could contribute up to 70% of SOA formation in the Los Angeles Air Basin despite accounting for only approximately 4% of total petrochemical product use (McDonald et al., 2018). Regional scale modeling that includes VCP emission inventories also shows improved agreement with ambient data compared to past models that historically did not consider VCP emissions (Seltzer et al., 2021; Pennington et al., 2021). However, because many of the chemicals comprising VCP emissions have not been studied in laboratory settings, their contribution to SOA formation is uncertain. Therefore, additional experimental work on VCPs is still needed.

Here, we evaluate the photochemistry of benzyl alcohol, a compound found prominently in VCPs. Benzyl alcohol is a C7 aromatic compound used in soaps and perfumes, and is also used as a solvent in the manufacture of paints, inks, lacquers, and epoxies (Wang, 2015). It was previous thought that benzyl alcohol had a modest SOA yield (< 10%) (McDonald et al., 2018). In a previous study, the aerosol mass yield of benzyl alcohol was found to have a high mass yield under a variety of conditions—even approaching unity (Charan et al., 2020; Jaoui et al., 2023).

Experimental studies, including kinetic experiments on benzyl alcohol, have identified the primary atmospheric oxidative pathway of benzyl alcohol to proceed via reaction with the OH radical (Bernard et al., 2013; Harrison et al., 2009). Harrison et al. calculated that benzyl alcohol reacts with OH at a rate of $(28 \pm 7) \times 10^{-12}$ cm^3 molecule $^{-1}$ s^{-1}. The reaction rate with O_3 was too slow to contribute to its oxidation in most environments (Harrison et al., 2009).

Previous experimental studies of benzyl alcohol identified several oxidation products including hydroxybenzyl alcohol (HBA) and benzaldehyde (Burkholder et al., 2017; Harrison et al., 2009; Bernard et al., 2013). A theoretical study on the mechanism of benzyl alcohol oxidation initiated by the hydroxy radicals (OH) also predicted the major oxidation pathways to form (Wang, 2015) benzaldehyde, i-hydroxybenzyl alcohol, and o-hydroxybenzyl alcohol. Other products observed in past experimental studies include ring-opening products, such as but-2-enedial and 6-hydroxy-5-oxohex-2-enal (Harrison et al., 2009), as well as C6 compounds, such as dihydroxy benzene (Bernard et al., 2013). These past experiments were conducted under high NO conditions. Yet, understanding chemical mechanisms and yields as a function of NO is important for understanding urban air quality as NO_x:VOC ratios have been shown to affect OH oxidation of VOCs and as NOx regimes continue to change in urban settings (Seinfeld et al., 2016; Parker et al., 2020).

In this study, we draw on past work which suggests HBA forms via addition of OH to the aromatic ring. We confirm products identified in past experimental studies and we confirm products predicted in the Wang (2015) theoretical study. We also report quantitative values for HBA, benzaldehyde, phenol, and hydroxy oxopentenal. We find the branching fraction for HBA, the primary oxidation product, is $\sim$ 29%. Benzaldehyde, the other main oxidation product, has a branching ratio of $\sim$ 21%.

2.2 Methods

Chamber experiments were conducted to elucidate the chemical mechanism of benzyl alcohol oxidation via OH. First-generation oxidation products were also used to identify important pathways to SOA formation.

Experimental Design

Gas-phase experiments were conducted in a $\sim$ 0.8 m^3 FEP Teflon-walled environmental chamber, henceforth referred to as Chamber G. The chamber was filled and evacuated multiple times with purified air prior to experiments. All experiments were run at room temperature ($\sim$ 22° C), low relative humidity ($<$ 10% RH), and ambient pressure ($\sim$ 1 atm). Benzyl alcohol (Sigma Millipore, ReagentPlus $\geq$ 99%) and was injected into the chamber by flowing warm air over over a measured amount of precursor deposited on a Pall Teflon filter.

For the high NO gas-phase experiments G2 and G4, methyl nitrite was used as the oxidant precursor. Methyl nitrite was added to the reactor by measuring the pressure of methyl nitrite into an evacuated round-bottom bulb and back-filling the remainder of the bulb volume with nitrogen. NO (1993±20 ppm NO in N_2, Matheson) was prepared in a similar manner. For high NO, particle-phase experiments, NO (506.9±10 ppm NO in N_2) was injected using a mass-flow controller (Sierra Instruments).

In experiments G1, G3, and G5, hydrogen peroxide (H_2O_2) (Sigma Millipore, 50 wt% in H_2O stabilized) was used as the OH precursor by injecting a known mass into a glass bulb and flowing purified air over the liquid droplets to add to the reactor. In particle-phase experiments, the H_2O_2 was heated in a water bath ($\sim$ 42°C) during injection.

Ultraviolet (UV) broadband lights centered around $\sim$ 350 nm were used as the light source for photooxidation (Light Sources, Inc.); oxidation duration was determined so that $\sim$ 10% of the precursor was reacted in gas-phase reactions. The j_{NO2} and j_{CH3ONO} for Chamber G are 4.4×10^{-3} s^{-1} and 1.1×10^{-3} s^{-1}, respectively.

Additional information about the oxidants is found in Appendix 2.4. A summary of experiments can be found in Table 2.1.

Table 2.1: Experimental summary

Expt. #	VOC	VOC Concentration (ppb)	[NO] (ppb)	Oxidant (ppb)
G1	Benzyl alcohol	539	1,000	H_2O_2 (2,000)
G2	Benzyl alcohol	46	500	CH_3ONO (300)
G3	Benzyl alcohol	523	50	H_2O_2 (2,000)
G4	Benzyl alcohol	60	44	CH_3ONO (370)
G5	Benzyl alcohol	538	0	H_2O_2 (2,000)

Instrumentation

NO_x was monitored using commercially available Teledyne NO_x M200 EU or T200 model. Additional instrumentation used in gas-phase and particle-phase experiments is described in the following sections.

A chemical ionization triple quadrupole mass spectrometer (CIMS) with a CF_3O^- reagent ion was used to monitor gas-phase compounds in particle-phase experiments. This set up has been described in detail elsewhere (Schwantes et al., 2017). In brief, the CIMS operates by reacting with the gas-phase compounds in the sample that have an electron affinity sufficient to bind with the reagent ion cluster (CF_3O^-). Sampled compounds that are acidic may also transfer a floride ion (F^-). The sample is then detected by a Varian 1200 triple quadrupole mass analyzer which measures masses from m/z = 50 to 330. A custom-built inlet to the CIMS was set at a constant temperature, 25° C.

Benzaldehyde, one of the primary products of benzyl alcohol OH oxidation, is not detectable using the CF_3O^- CIMS. Thus an HP 6890N gas chromatograph with a flame ionization detector (GC-FID) was used in in experiments G1, G3, and G5 to detect benzaldehyde. Experiments were run with a DB5 column. Information on the temperature profile and GC operation can be found in Appendix 2.6.

The GC-CIMS was used to monitor the gas phase precursors and subsequent photooxidation products. This experimental setup is described in detail elsewhere (Vasquez et al., 2018; Xu, Møller, Crounse, Kjaergaard, et al., 2020). Here, the GC-CIMS was operated in both negative mode using CF_3O^- and for experiments G2 and G4, in positive mode using NO^+. The chemistry involving CF_3O^- is the same as that described previously and in Appendix 2.5. In positive mode, NO^+

complexes with less acidic compounds and can be detected at [M+NO^+] (also described further in Appendix 2.5). A 2 m Restek RTX-1701 column was used for all experiments for better chromatographic resolution of certain isomers. GC samples were cryogenically trapped at −20° C on the column. Additional information on the GC-CIMS operation is in Appendix 2.6.

Calibrations

The sensitivities for analytes in the GC-CIMS were generally determined from standards prepared and quantified using Fourier transform infrared (FTIR) spectroscopy. The GC-FID and the CIMS in experiments P1 - P2 were calibrated by injecting the analyte of interest into a ∼ 100L Teflon pillow bag using the same injection method as described previously for Chamber G. The sample was then measured via a FTIR spectrometer with a pathlength of 19 cm. The reference FTIR spectra from the Pacific Northwest National Laboratory (PNNL) database were used to tabulate cross sections to determine exact concentrations Schwantes et al., 2017. The pillow bag was then diluted using dry N_2 and sampled to determine the instrumental sensitivity (Xu, Møller, Crounse, Otkjær, et al., 2019).

Several of the substrates involved in this study are relatively non-volatile, leading to challenges with quantitative transfer into and out of the FTIR cell. Therefore some of the GC-CIMS sensitivities were determined using calculated polarizabilities and dipole moments to determine the ion-collision rate of the analytes with the reagent ion relative to reference calibrants (Su et al., 1982; Garden et al., 2009). Additional information on this procedure can be found in Appendix 2.5.

Corrections

Secondary Chemistry

Oxidation products of benzyl alcohol react as they are formed. These losses were accounted in estimating the branching ratios of benzyl alcohol products which are reported in Table 2.3. Branching ratios (BR) were calculated as:

$$\mathrm{BR} = \mathrm{Y} \times \mathrm{CF}. \tag{2.1}$$

The gas-phase, time-dependent yield, Y, is calculated as the amount of oxidation product formed divided by the amount of precursor reacted. To solve for the correction factor, CF, a constant [OH] is assumed for the time-dependent product

concentration, which can be described as:

$$[\text{Product}]_t = [\text{BA}]_0 \times \frac{\text{Y} \times \text{k}_{\text{BA}}}{\text{k}_{\text{BA}} - \text{k}_{\text{Product}}} \times [\text{e}^{-\text{k}_{\text{Product}}[\text{OH}]\text{t}} - \text{e}^{-\text{k}_{\text{BA}}[\text{OH}]\text{t}}]. \quad (2.2)$$

The time-dependent concentration of benzyl alcohol is described as:

$$[\text{BA}]_t = [\text{BA}]_0 \times \text{e}^{-\text{k}_{\text{BA}}[\text{OH}]\text{t}}. \quad (2.3)$$

Therefore CF, the correction factor, is defined as:

$$CF = \frac{k_{BA} - k_{product}}{k_{BA}} \times \frac{1 - [BA]_t/[BA]_0}{([BA]_t/[BA]_0)^{k_{product}/k_{BA}} - ([BA]_t/[BA]_0)}. \quad (2.4)$$

This correction factor is described elsewhere in greater detail (Atkinson et al., 1982). The kinetic rate constants to solve for Eq. 5 can be found in Table 2.2. The correction factors were: $\sim 4-8\%$ for HBA; $< 0.2\%$ for phenol; $\sim 0.6-2\%$ for benzaldehyde; and $\sim 0.6-2.9\%$ for 5-hydroxy-4-oxo-2-pentenal.

Table 2.2: Kinetic rate constants used to determine the correction factors for branching ratio calculations.

Compound	k_{OH} ($\text{cm}^3\,\text{molec}^{-1}\,\text{s}^{-1}$)
Benzyl alcohol	$(2.8 \pm 0.7) \times 10^{-11*}$
Benzaldehyde	$(1.29 \pm 0.32) \times 10^{-11\dagger}$
Phenol	$(2.83 \pm 0.57) \times 10^{-11\dagger\dagger}$
Butenedial	$(3.45 \pm 0.34) \times 10^{-11**}$
Catechol	$(1.04\ pm) \times 10^{-10***}$

*Harrison et al., 2009 and Bernard et al., 2013 † Calvert et al., 2002. †† Rinke et al., 1984. ** Martín et al., 2013. *** (Pillar-Little et al., 2014). Note that for 5-hydroxy-4-oxo-2-pentenal, the k_{OH} for butenedial is used to calculate the correction factor.

Because we lacked an accurate measure of the kinetics of HBA, the signal of OH products from HBA was instead used. We observe a significant amount of catechol formed shortly after HBA formation. While a modest amount di-hydroxy benzyl alcohol forms, catechol is the primary oxidation product of HBA. We assume $\sim 100\%$ yield from HBA to catechol. Based on this assumption the correction for secondary chemistry for HBA is simply adding the amount of the catechol which itself has been corrected to account for secondary chemistry.

Vapor-Wall Loss

Vapor wall loss was examined by sampling benzyl alcohol (and products) prior to oxidation and post-oxidation. Vapor-wall loss periods were as long or on similar orders of magnitude as oxidation periods. We find that during these sample periods, the signal of oxidation products remains constant. Thus no vapor-wall loss correction is applied. This appears congruent with past work on quantifying benzyl alcohol products, as well as other work quantifying first-generation gas-phase products typically consider gas-phase wall loss to be negligible (Charan et al., 2020; Jaoui et al., 2023; Bernard et al., 2013; Harrison et al., 2009).

2.3 Results and Discussion

Gas-Phase Branching Ratios

Gas-phase products were identified in Experiments G1-3 (Table 2.1). The oxidation of first generation products were minimized by limiting the reaction of benzyl alcohol to $< 10\%$. The oxidation of benzyl alcohol forms C7 products, such as HBA and benzaldehyde. Additionally, we observed C6 (products such as phenol), as well as ring-opening products (such as 5-hydroxy-4-oxo-2-pentenal). A list of products and their corresponding CIMS chemistry can be found in Appendix 2.7.

Table 2.3: Results of gas-phase experiments

Experiment	Hydroxybenzyl Alcohol Branching Fraction	Benzaldehyde Branching Fraction	5-hydroxy-4-oxo-2-pentenal Branching Fraction	Phenol Fraction
1,000 ppb NO	(27 ± 14)%	(22 ± 6)%	(4.0 ± 1.6)%	(2.7 ± 1.2)%
500 ppb NO	(36 ± 18)%	(19 ± 12)%	(8.0 ± 2.7)%	(4.2 ± 1.9)%
50 ppb NO	(34 ± 17)%	(21 ± 6)%	(8.6 ± 3.0)%	(2.6 ± 1.2)%
44 ppb NO	(34 ± 17)%	(31 ± 20)%	(5.9 ± 2.3)%	(1.2 ± 0.58)%
0 ppb NO	(32 ± 16)%	(14 ± 4)%	(3.4 ± 1.4)%	(1.3 ± 0.58)%
Mean	(33 ± 16)%	(21 ± 10)%	(6.0 ± 2.3)%	(2.4 ± 1.1)%

While HBA is not currently included in the Master Chemical Mechanism (MCM) scheme, its formation is predicted and identified in past work on benzyl alcohol kinetics and mechanisms (Calvert et al., 2002; Bernard et al., 2013; Wang, 2015; Bloss et al., 2005; Jenkin et al., 2003). HBA forms via the addition of the OH radical to the aromatic ring. This leads to a radical intermediate which is stabilized by the electron delocalization of the remaining conjugated system. An additional hydrogen abstraction stabilizes the radical intermediate. We calculated the amount of HBA formed from benzyl alcohol oxidation from the gas-phase experiments conducted in Chamber G (Experiments G1 – G5 in Table 2.1). We found that the branching ratio of HBA to be invariable with [NO]. By averaging over all experiments and accounting for systematic errors, we find that the branching fraction of HBA averaged over different NO mixing ratios is $(33 \pm 16)\%$. The primary oxidation products of HBA appears to be catechol. See Section 2.3 for a more detailed discussion on how C6 compounds are formed. Dihydroxy benzyl alcohol was observed in modest quantities. We also observed masses that corresponded to fragmentation products observed in past studies or believed to form via theoretical calculations such as hydroxyoxopropanal. The mechanism for HBA formation and subsequent chemistry can be found in (See Figure 2.1).

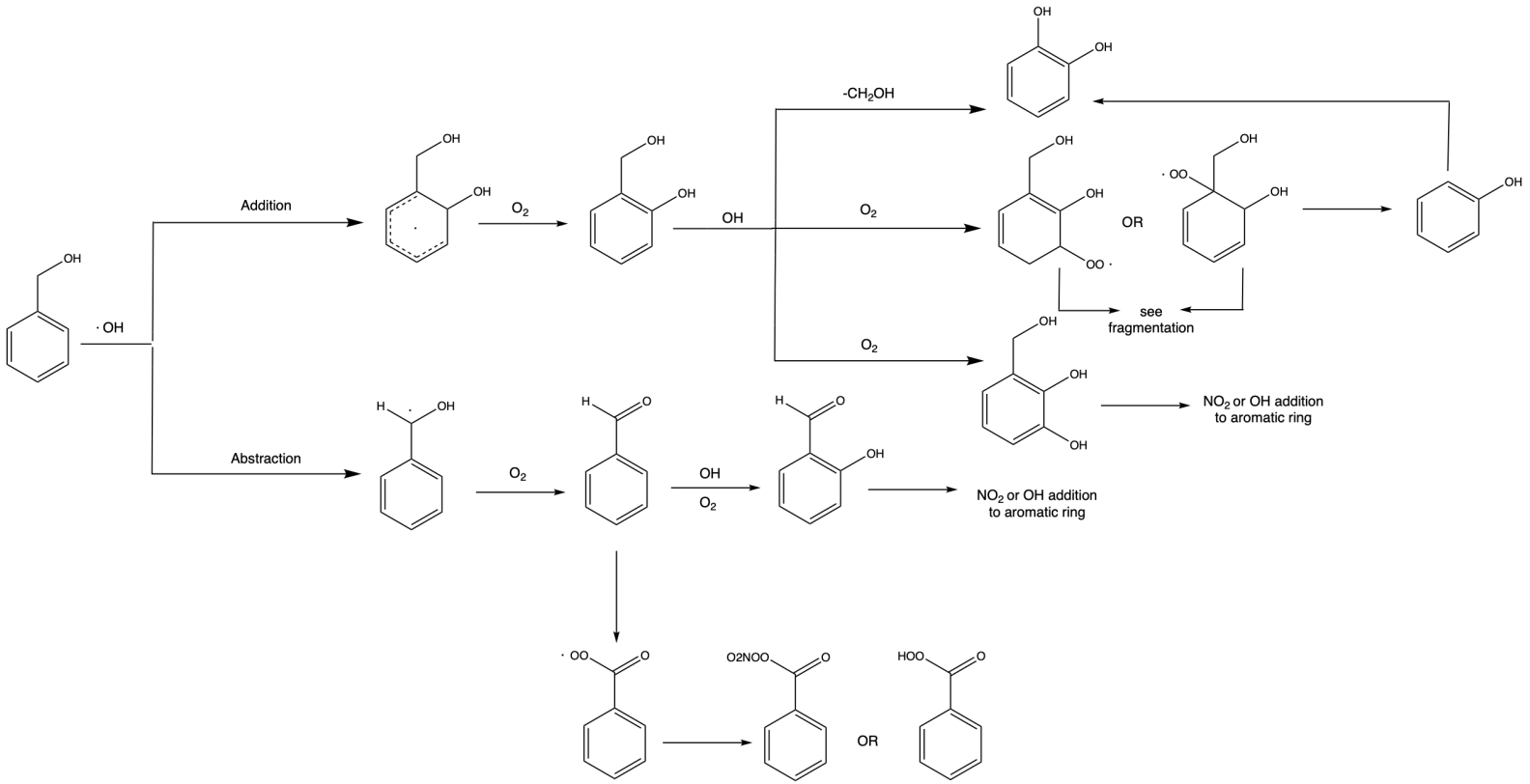

Figure 2.1: Primary reactive pathways for OH-initiated oxidation of benzyl alcohol.

Benzaldehyde forms via initial hydrogen abstraction from the CH_2OH group followed by addition of O_2 and subsequent loss of HO_2. Benzaldehyde was measured via NO^+ CIMS in experiments G2 and G4 and via GC-FID in experiments G1, G3, and G5. The NO^+ signal is highly water-dependent and therefore less stable than the CF_3O^- signal. Therefore, the error for the benzaldehyde branching fractions for experiments G2 and G4 is slightly larger than for experiments G1, G3, and G5. We estimated the branching fraction is $\sim$ 21% under high and low NO conditions, consistent with the expectation that this channel that should not have NO dependence when NO is less than several ppm (Allen et al., 2018). Bernard and coauthors quantified the branching fraction of benzaldehyde to be 25% (Bernard et al., 2013). Since benzaldehyde forms via a benzyl alcohol radical, the intermediate may stabilize to other closed shell products such as hydroperoxide benzaldehyde, and nitrate benzaldehyde. Benzaldehyde can also continue to react via OH addition to the aromatic ring to form products such as hydroxy benzaldehyde.

C6 Compounds

A previous study of the chemical composition of the SOA formed via OH oxidation of benzyl alcohol observed C6 compounds, such as nitrocatechol (Charan et al., 2020; Jaoui et al., 2023). In the present study, we observed nitrocatechol as well as other C6 compounds such as phenol and catechol. Past work has proposed C6 products can form from benzaldehyde oxidation (Figure 2.2) (Schwantes et al., 2017). Further reaction with NO leads to alkoxy benzene which can then stabilize to phenol. Phenol and other C6 products can also form by hydrogen abstraction from the CH_2OH group to form a formaldehyde leaving group. Wang (2015) estimated the barrier to decomposition is too high for significant formation of phenol, though predicted low yields of phenol via decomposition of the HBA radical adduct to form phenol and $\cdot CH_2OH$ which will react with O_2 to form formaldehyde. In the present study we observed small initial branching ratios of phenol $< 5\%$. We observed that the branching ratio of phenol decreases with decreasing NO, consistent with past studies showing the mechanism for phenol formation depends on NO mixing ratio (Xu, Møller, Crounse, Kjaergaard, et al., 2020).

We observed C6 compounds in both gas-phase and particle-phase experiments. Catechol, phenol, and other C6 aromatic compounds react rapidly with OH to form other oxygenated aromatic compounds ($\leq 2.7 \times 10^{-11}$ cm^3 molecule^{-1}s^{-1}) (Calvert et al., 2002). Thus, despite relatively low branching ratios of phenol in the first

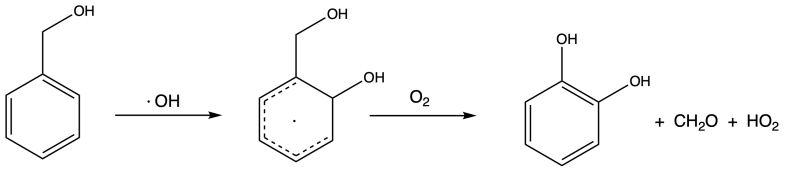

Figure 2.2: Phenol may form via the HBA radical adduct.

generation of this chemistry, we observed many C6 products in the aerosol. Wang (2015) also predicts a considerable yield of nitroaromatics. In high NO conditions, we observed nitrophenol in gas-phase and particle-phase experiments. Furthermore, in past work, nitrocatechol is identified as an important compound in the chemical composition of aerosol formed from benzyl alcohol oxidation (Charan et al., 2020).

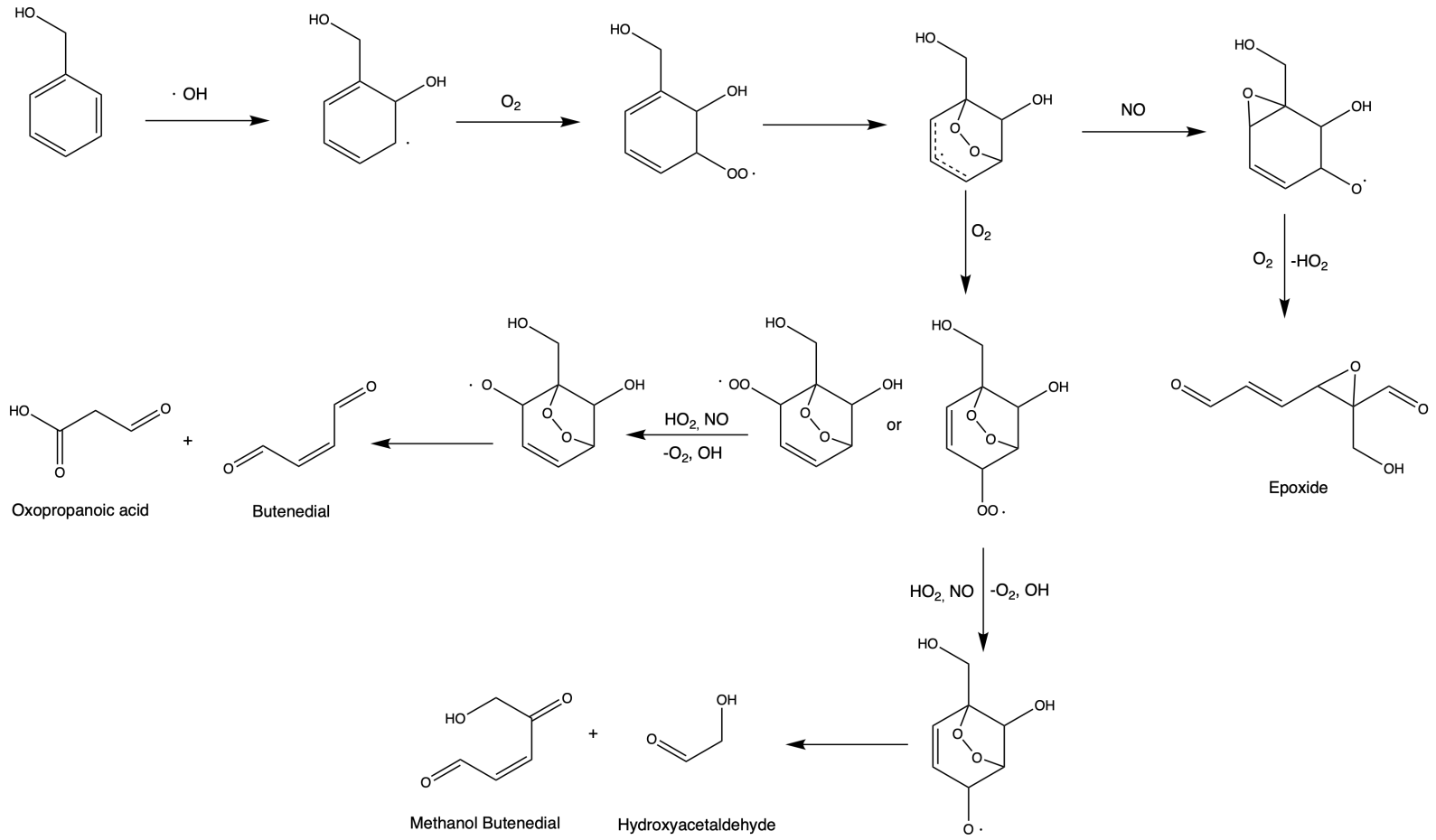

Figure 2.3: Following addition of OH to the aromatic ring, a bicyclic intermediate can form which can eventually lead to form fragmentation products. Here, we detect products with masses congruent with both the 5-hydroxy-4-oxo-2-pentenal and epoxide products.

Comparison With Past Work

Past studies have detected HBA and benzaldehyde from the oxidation of benzyl alcohol (Wang, 2015; Bernard et al., 2013; Harrison et al., 2009). Wang (2015) estimates the yield of o-HBA is 11% using theoretical estimates, while Bernard and coworkers estimate the yield is 21%; we found the branching fraction of HBA is $\sim$ 33%. Variations in our results compared to past studies are likely due to differences in initial conditions. Branching fractions are also affected by $[O_2]$, the initial benzyl alcohol mixing ratio, amount of benzyl alcohol reacted, OH exposure, and temperature, among other variables. In Bernard et al., 2013 starting benzyl alcohol mixing ratios ranged from $\sim$ 2000 ppb - 850 ppb, whereas in our system initial [benzyl alcohol] $<$ 100 ppb. If the system is allowed to react for sufficiently long, secondary chemistry can play an increasingly significant role. Unaccounted for secondary reactions may lead to an under-reporting of the HBA branching ratio, especially in longer oxidation experiments. Additionally, to our knowledge, no yield studies have been previously conducted for this system in the absence of NO.

We observed only one isomer of HBA which we assume to be the *ortho* product. This assignment is based on past work that suggests the *ortho* position is a major product in aromatic oxidation chemistry by OH (Harrison et al., 2009; Finlayson-Pitts, Barbara et al., 1986; Baltaretu et al., 2009). Similarly, Wang, 2015 predicted a single stable isomer of HBA, *ortho*. If additional HBA isomers existed in our system, it is likely they would have eluted at higher temperatures than were allowed by the current GC temperature profiles and were therefore undetected. However, secondary isomer formation is typically considered to be minor in other aromatic systems (Finlayson-Pitts, Barbara et al., 1986; Baltaretu et al., 2009).

Bernard et al., 2013 also reported a benzaldehyde yield of (25 ± 4)%, which was used as input to the computations performed in Wang 2015, while Harrison and Wells report a yield of 24% (no error provided) (Bernard et al., 2013; Wang, 2015; Harrison et al., 2009). We report a benzladehyde an averaged branching fraction of (21 ± 10)%, in close agreement with past work.

Conclusion

Benzyl alcohol oxidizes via OH to primarily form HBA and benzaldehyde. Significant additional chemistry occurred via endocylization following addition of oxygen to fragmentation products such as 5-hydroxy-4-oxo-2-pentenal and butadiene. We found that [NO] does not have an effect on product yields for HBA, benzaldehyde,

and 5-hydroxy-4-oxo-2-pentenal. HBA was the dominant first-generation product with a branching ratio of $\sim$ 33% over a range of NO conditions. The branching ratio of benzaldehyde is estimated to be $\sim$ 21%.

Both HBA and benzaldehyde pathways go on to form highly oxygenated gas-phase products. HBA oxidation leads to the formation of products such as dihydroxybenzyl alcohol, while similarly, benzaldehyde oxidation forms products such as dihydroxy benzoic acid. These products indicate that subsequent OH addition to the aromatic ring occured in both pathways. Both the addition and hydrogen abstraction routes may have also contribute to the formation of C6 products.

APPENDIX

2.4 Experimental Conditions

CH_3ONO (synthesized following Taylor et al. (1980)), and NO (1993±20 ppmv, Matheson) were injected into the Chamber G (~ 800 L) in a similar fashion. The analyte is introduced to an evacuated 0.5 L glass bulb and is serially diluted with N_2 until the desired mixing ratio is achieved. CH_3ONO was quantified via FTIR spectroscopy using tabulated cross section prior to being injected into Chamber G. Ultraviolet lights (Sylvania) centered around 350 nm were used. The measured j_{CH3ONO} and inferred j_{NO2} from these lights are $1.1 \times 10^{-3} s^{-1}$ and $4.4 \times 10^{-3} s^{-1}$, respectively.

2.5 CIMS Calibration and Instrument Sensitivity

The CIMS operates by flowing the reagent ion source (CF_3OOCF_3 in negative mode and $NO \cdot H_2O^+$ in positive mode) through a radioactive source (^{210}Po), generating the reagent ions. In negative mode, cluster ions (Eq. 2.5) or transfer ions (Eq. 2.6) are produced. CF_3O^- CIMS chemistry is documented extensively in past studies (Vasquez et al., 2018; St. Clair et al., 2010; Crounse et al., 2006). In short, the CF_3O^- ion is sensitive to a variety of atmospherically-relevant oxygenated species.

$$M + CF_3O \leftrightarrow M \cdot CF_3O^- \tag{2.5}$$

$$M + CF_3O \rightarrow M{-}H^- \cdot HF + CF_2O \tag{2.6}$$

In positive mode, $NO \cdot H_2O^+$ is produced (Eq. 2.7). Ambient N_2 and H_2O react with NO. The $NO \cdot H_2O^+$ tends to bind to less oxygenated species including carbonyls such as benzaldehyde.

$$N_2{}^+ + NO \rightarrow NO^+ + N_2 \tag{2.7}$$

$$NO^+ + H_2O^+ \leftrightarrow M \cdot NO^+ + H_2O \tag{2.8}$$

The GC-CIMS and GC-FID in gas-phase experiments was calibrated for D5 phenol (pentadeuterated phenol) and benzaldehyde, respectively. For the latter preparation, benzaldehyde was injected into a ~ 100 L Teflon pillow bag using the same injection method as described previously. The sample was then measured via a Fourier transform infrared (FTIR) spectrometer with a path length of 19 cm. The reference FTIR spectrum from the Pacific Northwest National Laboratory (PNNL) database

Compound	Average Dipole (D) at 298 K	Polarizability (Å^3)
Phenol	1.828	10.07
Catechol	2.364	10.76
o-Hydroxy benzyl alcohol (o-HBA)	2.109	12.63
p-Hydroxy benzyl alcohol (p-HBA)	1.286	12.76
Benzyl alcohol	1.457	1.780
Z-5OH-4CO-pent-2-enal	3.072	10.55
E-5OH-4CO-pent-2-enal	2.015	10.80
o-Hydroxy benzaldehyde	3.008	12.64

Table 2.4: Quantum calculations of dipole moments and polarzabilities (at the B3LYP/cc-pVTZ level).

was used to tabulate cross sections to determine the exact concentration of the calibrant (Schwantes et al., 2017). The pillow bag was then diluted using dry N_2 and sampled to determine the instrumental sensitivity.

To estimate the sensitivities for other less volatile analytes, the ion-molecule collision rate was used relative to D5 phenol. o-HBA, p-HBA, 5-hydroxy-4-oxo-2-pentenal, catechol, and benzyl alcohol were calibrated in this way. Average dipole moments at 298 K and polarizabilities (at B3LYP/cc-pVTZ level) were calculated for all analytes of interest (Table 2.4). These parameters were then used to determine the ion-collision rate between analytes and reagent ion as described in Su et al., 1982. This rate is linearly related to the fraction ionized of each analyte (Murphy et al., 2023). These calculations are then used to determine the compound-specific sensitivity to the CIMS signal by relating the ratio of parameters in Table 2.4 to the ratio of instrument sensitivity relative to the reference calibrant (Garden et al., 2009).

Catechol and D5 phenol were calibrated using permeation tubes which were weighed to determine the mass loss of the analyte. The permeation tubes were heated to 40°C and then flowed directly into the flow-tube of the GC-CIMS. The known amount substrate was then correlated to signal on the GC-CIMS to determine its sensitivity. For these measurements, we assume the sensitivity of D5 phenol to be the same as the sensitivity of phenol.

2.6 GC Operation

In gas-phase experiments, analyte samples were cryogenically trapped in the GC-CIMS at ~ -20°C for 10 mins using liquid CO_2. The sample was eluted through the GC using a ramp of 10°C/min to 55°C and then 2.5°C/min to 130°C. The slower

ramp rate from 55 – 130°C was used because most oxidation products eluted at this time and using a slower ramp ensured relevant products were sufficiently separated. When GC scans were not being taken, the CIMS sampled directly from the reaction chamber.

2.7 Oxidation Products Detected

The following table summarizes masses detected by the GC-CIMS in gas-phase experiments (G1 - G3). While some products were identified using authentic standards, other assignments are based on masses detected and our chemical understanding of this and other aromatic systems.

VOC Compound (m/z)	Structure	Formula	Observed m/z and Reagent Ion
Benzyl alcohol (108)		$C_6H_5CH_2OH$	193 (CF_3O^-)
Benzaldehyde (106)		$C_6H_5C(O)$	136 (NO^+)
Hydroxybenzyl alcohol (124)		$C_6H_4OHCH_2OH$	143 (F^-) and 209 (CF_3O^-)
Dihydroxybenzyl alcohol (140)		$C_6H_4OHOHCH_2OH$	225 (CF_3O^-)
Phenol (94)		C_6H_5OH	113 (F^-) and 179 (CF_3O^-)
Catechol (110)		C_6H_4OHOH	129 (F^-) and 195 (CF_3O^-)
Hydroxymethylbutenedial (114)	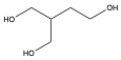	$C_5O_3H_6$	199 (CF_3O^-)
Nitrophenol (139)	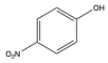	$C_6H_5NO_3$	158 (F^-)
Dihydroxybenzoic acid (154)		$C_6H_3OHOHC(O)OH$	173 (F^-)
Bicyclic aromatic (219)	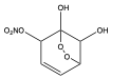	$C_6O_7NH_9$	173 (F^-)
Tetrahydroxy benzene (142)	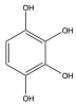	$C_6H_6O_4$	161 (F^-)
Glyoxal (58)		$C_2H_2O_2$	88 (NO^+)
Formic acid (46)		CH_2O_2	86 (NO^+)
Benzoquinone (108)		$C_6H_4O_2$	138 (NO^+)
Oxopentanal (100)	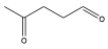	$C_5H_8O_2$	140 (NO^+)
Butenedial (84)		$C_4H_4O_2$	114 (NO^+)
Oxopropanoic acid (88)		$C_3H_4O_3$	173 (CF_3O^-)
Methanol butenedial (114)		$C_5O_3H_6$	199 (CF_3O^-)
Hydroxyacetaldehyde (60)		$C_2O_2H_4$	145 (CF_3O^-)

Table 2.5: Compound assignments from CIMS data. Note that several of the compounds listed have many isomeric structures though only one may be listed as an example.

2.8 Estimation of Uncertainty

In gas phase experiments, the major source of error in our calculation of yields comes from the relative sensitivity of the product concentration as measured by their respective instruments. A part of the reported error is also determined by calculating the standard deviation of signal variation. This varies from compound to compound and is also dependent on the reagent gas used. Uncertainty in quantifying the relative signals in positive and negative. Based on this, we estimate the error for compounds detected by the GC-CIMS is $\sim 63\%$. Phenol was directly calibrated for branching ratio calculations, therefore the estimated uncertainty for phenol is 21%.

References

Allen, Hannah M., John D. Crounse, Kelvin H. Bates, Alexander Paichung Teng, Mitchell P. Krawiec-Thayer, Jean C. Rivera-Rios, Frank N. Keutsch, Jason M. St. Clair, Thomas F. Hanisco, Kristian H. Møller, Henrik G. Kjaergaard, and Paul O. Wennberg (Aug. 2018). "Kinetics and Product Yields of the OH Initiated Oxidation of Hydroxymethyl Hydroperoxide". en. In: *The Journal of Physical Chemistry A* 122.30, pp. 6292–6302. ISSN: 1089-5639, 1520-5215. DOI: 10.1021/acs.jpca.8b04577. URL: https://pubs.acs.org/doi/10.1021/acs.jpca.8b04577 (visited on 05/30/2024).

Atkinson, Roger, Sara M. Aschmann, Willlam P.L. Carter, Arthur M. Winer, and James N. Pitts (Nov. 1982). "Alkyl nitrate formation from the NO-air photooxidations of C2-C8 n-alkanes". en. In: *Journal of Physical Chemistry, The* 86:23, p. 7. URL: https://doi.org/10.1021/j100220a022.

Baltaretu, Cristian O., Eben I. Lichtman, Amelia B. Hadler, and Matthew J. Elrod (Jan. 2009). "Primary atmospheric oxidation mechanism for toluene". en. In: *The Journal of Physical Chemistry A* 113.1, pp. 221–230. ISSN: 1089-5639, 1520-5215. DOI: 10.1021/jp806841t. URL: https://pubs.acs.org/doi/10.1021/jp806841t (visited on 03/29/2023).

Bernard, François, Isabelle Magneron, Grégory Eyglunent, Véronique Daële, Timothy J. Wallington, Michael D. Hurley, and Abdelwahid Mellouki (Apr. 2013). "Atmospheric chemistry of benzyl alcohol: kinetics and mechanism of reaction with OH radicals". en. In: *Environmental Science & Technology* 47.7, pp. 3182–3189. ISSN: 0013-936X, 1520-5851. DOI: 10.1021/es304600z. URL: http://pubs.acs.org/doi/10.1021/es304600z (visited on 05/27/2019).

Bloss, C., V. Wagner, M.E. Jenkin, R. Volkamer, W.J. Bloss, J D Lee, D E Heard, K Wirtz, M Martin-Reviejo, G Rea, J C Wenger, and M J Pilling (2005). "Development of a detailed chemical mechanism (MCMv3.1) for the atmospheric oxidation of aromatic hydrocarbons". en. In: *Atmospheric Chemistry and Physics*.

Burkholder, James B., Jonathan P. D. Abbatt, Ian Barnes, James M. Roberts, Megan L. Melamed, Markus Ammann, Allan K. Bertram, Christopher D. Cappa, Annmarie G. Carlton, Lucy J. Carpenter, John N. Crowley, Yael Dubowski, Christian George, Dwayne E. Heard, Hartmut Herrmann, Frank N. Keutsch, Jesse H. Kroll, V. Faye McNeill, Nga Lee Ng, Sergey A. Nizkorodov, John J. Orlando, Carl J. Percival, Bénédicte Picquet-Varrault, Yinon Rudich, Paul W. Seakins, Jason D. Surratt, Hiroshi Tanimoto, Joel A. Thornton, Zhu Tong, Geoffrey S. Tyndall, Andreas Wahner, Charles J. Weschler, Kevin R. Wilson, and Paul J. Ziemann (Mar. 2017). "The essential role for laboratory studies in atmospheric chemistry". en. In: *Environmental Science & Technology* 51.5, pp. 2519–2528. ISSN: 0013-936X, 1520-5851. DOI: 10.1021/acs.est.6b04947. URL: https://pubs.acs.org/doi/10.1021/acs.est.6b04947 (visited on 04/15/2020).

Calvert, Jack G., Atkinson, Roger, Becker, Karl H., Kamens, Richard M., John H. Seinfeld, Wallington, Timothy J., and Yarwood, Greg (2002). *The mechanism of atmospheric oxidation of aromatic hydrocarbons*. New York, New York: Oxford University Press.

Charan, Sophia M., Reina S. Buenconsejo, and John H. Seinfeld (Nov. 2020). "Secondary organic aerosol yields from the oxidation of benzyl alcohol". en. In: *Atmospheric Chemistry and Physics* 20.21, pp. 13167–13190. ISSN: 1680-7324. DOI: 10.5194/acp-20-13167-2020. URL: https://acp.copernicus.org/articles/20/13167/2020/ (visited on 10/26/2021).

Coggon, Matthew M., Georgios I. Gkatzelis, Brian C. McDonald, Jessica B. Gilman, Rebecca H. Schwantes, Nader Abuhassan, Kenneth C. Aikin, Mark F. Arend, Timothy A. Berkoff, Steven S. Brown, Teresa L. Campos, Russell R. Dickerson, Guillaume Gronoff, James F. Hurley, Gabriel Isaacman-VanWertz, Abigail R. Koss, Meng Li, Stuart A. McKeen, Fred Moshary, Jeff Peischl, Veronika Pospisilova, Xinrong Ren, Anna Wilson, Yonghua Wu, Michael Trainer, and Carsten Warneke (Aug. 2021). "Volatile chemical product emissions enhance ozone and modulate urban chemistry". en. In: *Proceedings of the National Academy of Sciences* 118.32, e2026653118. ISSN: 0027-8424, 1091-6490. DOI: 10.1073/pnas.2026653118. URL: https://pnas.org/doi/full/10.1073/pnas.2026653118 (visited on 05/16/2022).

Crounse, John D., Karena A. McKinney, Alan J. Kwan, and Paul O. Wennberg (Oct. 2006). "Measurement of gas-phase hydroperoxides by chemical ionization mass spectrometry". en. In: *Analytical Chemistry* 78.19, pp. 6726–6732. ISSN: 0003-2700, 1520-6882. DOI: 10.1021/ac0604235. URL: https://pubs.acs.org/doi/10.1021/ac0604235 (visited on 03/15/2024).

Finlayson-Pitts, Barbara and Pitts, James N. Jr. (1986). *Atmospheric chemistry: fundamentals and experimental techniques*. United States: Wiley-Interscience. ISBN: 0-471-88227-5.

Garden, Anna L., Fabien Paulot, John D. Crounse, Isobel J. Maxwell-Cameron, Paul O. Wennberg, and Henrik G. Kjaergaard (May 2009). "Calculation of conformationally weighted dipole moments useful in ion–molecule collision rate estimates". en. In: *Chemical Physics Letters* 474.1-3, pp. 45–50. ISSN: 00092614. DOI: 10.1016/j.cplett.2009.04.038. URL: https://linkinghub.elsevier.com/retrieve/pii/S0009261409004679 (visited on 03/13/2024).

Harrison, Joel C. and J.R. Wells (Feb. 2009). "Gas-phase chemistry of benzyl alcohol: Reaction rate constants and products with OH radical and ozone". en. In: *Atmospheric Environment* 43.4, pp. 798–804. ISSN: 13522310. DOI: 10.1016/j.atmosenv.2008.11.001. URL: https://linkinghub.elsevier.com/retrieve/pii/S1352231008010297 (visited on 06/03/2019).

Jaoui, Mohammed, Kenneth S. Docherty, Michael Lewandowski, and Tadeusz E. Kleindienst (Apr. 2023). "Yields and molecular composition of gas-phase and

secondary organic aerosol from the photooxidation of the volatile consumer product benzyl alcohol: formation of highly oxygenated and hydroxy nitro-aromatic compounds". en. In: *Atmospheric Chemistry and Physics* 23.8, pp. 4637–4661. ISSN: 1680-7324. DOI: 10.5194/acp-23-4637-2023. URL: https://acp.copernicus.org/articles/23/4637/2023/ (visited on 05/24/2023).

Jenkin, M.E., S.M. Saunders, V. Wagner, and M.J. Pilling (2003). "Protocol for the development of the Master Chemical Mechanism, MCM v3 (Part B): Tropospheric degradation of aromatic volatile organic compounds". en. In: *Atmospheric Chemistry and Physics*.

Martín, Pilar, Beatriz Cabañas, Inmaculada Colmenar, María Sagrario Salgado, Florentina Villanueva, and Araceli Tapia (May 2013). "Reactivity of E-butenedial with the major atmospheric oxidants". en. In: *Atmospheric Environment* 70, pp. 351–360. ISSN: 13522310. DOI: 10.1016/j.atmosenv.2013.01.041. URL: https://linkinghub.elsevier.com/retrieve/pii/S1352231013000666 (visited on 05/09/2023).

McDonald, Brian C., Joost A. de Gouw, Jessica B. Gilman, Shantanu H. Jathar, Ali Akherati, Christopher D. Cappa, Jose L. Jimenez, Julia Lee-Taylor, Patrick L. Hayes, Stuart A. McKeen, Yu Yan Cui, Si-Wan Kim, Drew R. Gentner, Gabriel Isaacman-VanWertz, Allen H. Goldstein, Robert A. Harley, Gregory J. Frost, James M. Roberts, Thomas B. Ryerson, and Michael Trainer (Feb. 2018). "Volatile chemical products emerging as largest petrochemical source of urban organic emissions". en. In: *Science* 359.6377, pp. 760–764. ISSN: 0036-8075, 1095-9203. DOI: 10.1126/science.aaq0524. URL: http://www.sciencemag.org/lookup/doi/10.1126/science.aaq0524 (visited on 10/12/2018).

Murphy, Sara E., John D. Crounse, Kristian H. Møller, Samir P. Rezgui, Nicholas J. Hafeman, James Park, Henrik G. Kjaergaard, Brian M. Stoltz, and Paul O. Wennberg (2023). "Accretion product formation in the self-reaction of ethene-derived hydroxy peroxy radicals". en. In: *Environmental Science: Atmospheres* 3.5, pp. 882–893. ISSN: 2634-3606. DOI: 10.1039/D3EA00020F. URL: http://xlink.rsc.org/?DOI=D3EA00020F (visited on 09/06/2023).

Parker, H. A., S. Hasheminassab, J. D. Crounse, C. M. Roehl, and P. O. Wennberg (Dec. 2020). "Impacts of Traffic Reductions Associated With COVID-19 on Southern California Air Quality". en. In: *Geophysical Research Letters* 47.23. ISSN: 0094-8276, 1944-8007. DOI: 10.1029/2020GL090164. URL: https://onlinelibrary.wiley.com/doi/10.1029/2020GL090164 (visited on 05/22/2023).

Pennington, Elyse A., Karl M. Seltzer, Benjamin N. Murphy, Momei Qin, John H. Seinfeld, and Havala O. T. Pye (Dec. 2021). "Modeling secondary organic aerosol formation from volatile chemical products". en. In: *Atmospheric Chemistry and Physics* 21.24, pp. 18247–18261. ISSN: 1680-7324. DOI: 10.5194/acp-21-18247-2021. URL: https://acp.copernicus.org/articles/21/18247/2021/ (visited on 05/19/2022).

Pillar-Little, Elizabeth A., Robert C. Camm, and Marcelo I. Guzman (Dec. 2014). "Catechol oxidation by ozone and hydroxyl radicals at the air–water interface". en. In: *Environmental Science & Technology* 48.24, pp. 14352–14360. ISSN: 0013-936X, 1520-5851. DOI: 10.1021/es504094x. URL: https://pubs.acs.org/doi/10.1021/es504094x (visited on 05/28/2024).

Rinke, Monika and Cornelius Zetzsch (Jan. 1984). "Rate Constants for the Reactions of OH Radicals with Aromatics: Benzene, Phenol, Aniline, and 1,2,4-Trichlorobenzene". en. In: *Berichte der Bunsengesellschaft für physikalische Chemie* 88.1, pp. 55–62. ISSN: 00059021. DOI: 10.1002/bbpc.19840880114. URL: https://onlinelibrary.wiley.com/doi/10.1002/bbpc.19840880114 (visited on 05/09/2023).

Schwantes, Rebecca H., Katherine A. Schilling, Renee C. McVay, Hanna Lignell, Matthew M. Coggon, Xuan Zhang, Paul O. Wennberg, and John H. Seinfeld (Mar. 2017). "Formation of highly oxygenated low-volatility products from cresol oxidation". en. In: *Atmospheric Chemistry and Physics* 17.5, pp. 3453–3474. ISSN: 1680-7324. DOI: 10.5194/acp-17-3453-2017. URL: https://www.atmos-chem-phys.net/17/3453/2017/ (visited on 12/14/2018).

Seinfeld, John H. and Spyros N. Pandis (2016). *Atmospheric chemistry and physics: From air pollution to climate change*. en. Third edition. Hoboken, New Jersey: John Wiley & Sons. ISBN: 978-1-119-22116-6 978-1-119-22117-3.

Seltzer, Karl M., Elyse Pennington, Venkatesh Rao, Benjamin N. Murphy, Madeleine Strum, Kristin K. Isaacs, and Havala O. T. Pye (Mar. 2021). "Reactive organic carbon emissions from volatile chemical products". en. In: *Atmospheric Chemistry and Physics* 21.6, pp. 5079–5100. ISSN: 1680-7324. DOI: 10.5194/acp-21-5079-2021. URL: https://acp.copernicus.org/articles/21/5079/2021/ (visited on 11/29/2022).

St. Clair, Jason M., David C. McCabe, John D. Crounse, Urs Steiner, and Paul O. Wennberg (Sept. 2010). "Chemical ionization tandem mass spectrometer for the *in situ* measurement of methyl hydrogen peroxide". en. In: *Review of Scientific Instruments* 81.9, p. 094102. ISSN: 0034-6748, 1089-7623. DOI: 10.1063/1.3480552. URL: https://pubs.aip.org/aip/rsi/article/353641 (visited on 05/09/2023).

Su, Timothy and Walter J. Chesnavich (May 1982). "Parametrization of the ion-polar molecule collision rate constant by trajectory calculations". en. In: *The Journal of Chemical Physics* 76.10, pp. 5183–5185. ISSN: 0021-9606, 1089-7690. DOI: 10.1063/1.442828. URL: https://pubs.aip.org/jcp/article/76/10/5183/89898/Parametrization-of-the-ion-polar-molecule (visited on 03/13/2024).

Taylor, W.D., T.D. Allston, M.J. Moscato, G.B. Fazekas, R. Kozlowski, and G.A. Takacs (Apr. 1980). "Atmospheric photodissociation lifetimes for nitromethane, methyl nitrite, and methyl nitrate". In: *International Journal of Chemical Kinetics* 12.4, pp. 231–240. URL: https://doi.org/10.1002/kin.550120404.

Vasquez, Krystal T., Hannah M. Allen, John D. Crounse, Eric Praske, Lu Xu, Anke C. Noelscher, and Paul O. Wennberg (2018). "Low-pressure gas chromatography with chemical ionization mass spectrometry for quantification of multifunctional organic compounds in the atmosphere". en. In: *Atmospheric Measurement Techniques* 11, pp. 6815–6832. DOI: 10.5194/amt-2018-223. URL: https://www.atmos-meas-tech-discuss.net/amt-2018-223/amt-2018-223.pdf (visited on 12/13/2019).

Wang, Liming (May 2015). "The Atmospheric Oxidation Mechanism of Benzyl Alcohol Initiated by OH Radicals: The Addition Channels". en. In: *ChemPhysChem* 16.7, pp. 1542–1550. ISSN: 14394235. DOI: 10.1002/cphc.201500012. URL: http://doi.wiley.com/10.1002/cphc.201500012 (visited on 06/03/2019).

Xu, Lu, Kristian H. Møller, John D. Crounse, Henrik G. Kjaergaard, and Paul O. Wennberg (Nov. 2020). "New Insights into the Radical Chemistry and Product Distribution in the OH-Initiated Oxidation of Benzene". en. In: *Environmental Science & Technology* 54.21, pp. 13467–13477. ISSN: 0013-936X, 1520-5851. DOI: 10.1021/acs.est.0c04780. URL: https://pubs.acs.org/doi/10.1021/acs.est.0c04780 (visited on 01/31/2022).

Xu, Lu, Kristian H. Møller, John D. Crounse, Rasmus V. Otkjær, Henrik G. Kjaergaard, and Paul O. Wennberg (Feb. 2019). "Unimolecular Reactions of Peroxy Radicals Formed in the Oxidation of alpha-Pinene and beta-Pinene by Hydroxyl Radicals". en. In: *The Journal of Physical Chemistry A* 123.8, pp. 1661–1674. ISSN: 1089-5639, 1520-5215. DOI: 10.1021/acs.jpca.8b11726. URL: https://pubs.acs.org/doi/10.1021/acs.jpca.8b11726 (visited on 04/06/2020).

Chapter 3

CHEMICAL COMPOSITION AND FORMATION OF BENZYL-ALCOHOL-DERIVED SOA

Charan, Sophia M., **Buenconsejo, Reina S.**, and John H. Seinfeld (Nov. 10, 2020). "Secondary organic aerosol yields from the oxidation of benzyl alcohol". In: *Atmospheric Chemistry and Physics* 20.21, pp. 13167–13190. ISSN: 1680-7324. DOI: 10.5194/acp-20-13167-2020. URL: https://acp.copernicus.org/articles/20/13167/2020/.

Buenconsejo, Reina S., Sophia M. Charan, John H. Seinfeld, and Paul O. Wennberg (Nov. 8, 2023). "Quantifying primary oxidation products in the OH-initiated reaction of benzyl alcohol". In: DOI: 10.5194/egusphere-2023-2483. URL: https://egusphere.copernicus.org/preprints/2023/egusphere-2023-2483/.

Abstract

Understanding the chemical composition and formation of secondary organic aerosol (SOA) from volatile chemical products (VCPs) such as benzyl alcohol is critically important to understanding the landscape of modern air quality. This chapter examines the SOA formed by benzyl alcohol oxidation. First, molecular composition of the SOA formed from benzyl alcohol is investigated using filter samples analyzed by an ultra-performance liquid chromatography/electrospray ionization quadrupole time-of-flight mass spectrometer (UPLC/ESI-Q-TOF-MS, henceforth referred to as UPLC). This analysis helps elucidate the oxidation products that result in SOA formation. This chapter also reports the SOA yield of benzyl alcohol, as well as the SOA yields of the first generation oxidation products of benzyl alcohol, benzladehyde and hydroxybenzyl alcohol. This work illustrates the relative importance of different chemical pathways to SOA formation. Insights from this chapter can elucidate our understanding of the chemical composition and SOA contribution of other aromatic systems.

3.1 Introduction

Benzyl alcohol is a C7 aromatic compound that is found ubiquitously in VCPs such as soaps, inks, paints and, correspondingly, indoor air (Wang, 2015). Recent

work has identified the importance of volatile chemical products (VCPs) in urban environments, with one recent work estimating that VCPs makeup $\sim$ 61% of all petrochemical-derived SOA potential (McDonald et al., 2018). Yet gaps in modeling and observational data persist (Pennington et al., 2021). This is likely in part due to incomplete characterization of key VCP components. Thus, it is important to characterize the effects of VCP on atmospheric secondary organic aerosol (SOA) and its formation in order to better resolve discrepancies between SOA observations and models.

A body of work illustrates the importance of aromatics to SOA formation (Henze et al., 2008). Many atmospherically-relevant aromatics, such as benzene, toluene, phenol, among others, have been well studied (Finlayson-Pitts, Barbara et al., 1986, Calvert et al., 2002, Ng et al., 2007, Vereecken, 2019). Yet, some key aromatics remain under characterized. While past work has estimated or modeled the benzyl alcohol system, key uncertainties exist. For example, one multi-generational oxidation model estimated a modest yield benzyl alcohol (McDonald et al., 2018). Using the Statistical Oxidation Model, McDonald et al. calculated that benzyl alcohol has an SOA yield of 0.09 under high NO_x conditions. However, in other work the SOA yield of benzyl alcohol was estimated to be $\sim$ 0.3 in a mixture of compounds under high NO conditions. Thus the need for characterizing SOA yields and SOA chemical composition in the benzyl alcohol system is needed.

The goal of this chapter is to draw on the chemistry discussed in Chapter 2 to inform an analysis of the SOA formation from benzyl alcohol oxidation. This work characterizes the SOA yield of benzyl alcohol in an environmental chamber in tandem with off-line chemical analysis techniques such as ultra-performance liquid chromatography in tandem with mass spectrometry (UPLC-MS). Based on the work in Chapter 2, this chapter also explores the SOA yields of the primary first-generation oxidation products of benzyl alcohol, namly hydroxybenzyl alcohol (HBA) and benzaldehyde. We observe that HBA has a high SOA yield: for the reaction times in this study, approaching unity. HBA, therefore, likely contributes to the high SOA yield of benzyl alcohol which under some conditions can also approach unity. The goal of this chapter is to draw on the chemistry discussed in Chapter 2 to inform an analysis of the SOA formation from benzyl alcohol oxidation. This work characterizes the SOA yield of benzyl alcohol in an environmental chamber in tandem with off-line chemical analysis techniques such as ultra-performance liquid chromatography in tandem with mass spectrometry (UPLC-MS). Characterizing

the chemical composition of the SOA formed helps one understand the relative importance of gas-phase products (as identified in Chapter 2) to SOA partitioning. This analysis can also help inform potential toxicity of SOA. Based on the work in Chapter 2, this chapter also explores the SOA yields of the primary first-generation oxidation products of benzyl alcohol, namely hydroxybenzyl alcohol (HBA) and benzaldehyde. The goal of the additional SOA yield experiments is to understand the relative contribution to SOA formation from the two chemical pathways.

3.2 Methods

Experiments described in this chapter were conducted in a 17.9 m^3 FEP Teflon-lined environmental chamber. Prior to each experiment, the chamber was continuously flushed for > 24 h with clean air.

The OH radical source was H_2O_2 which was injected by flowing 5 Lpm N_2 over aliquots of H_2O_2 while in a 42°C water bath. Ultraviolet (UV) lights centered around 350 nm photolyzed the H_2O_2. The j_{NO_2} and $j_{H_2O_2}$ of the environmental chamber are measured to be 4.4×10^{-3} s^{-1} and 3.2×10^{-6} s^{-1}, respectively, using methods described elsewhere (Zafonte et al., 1977).

Benzyl alcohol and benzaldehyde (Sigma Aldrich ReagentPlus, ≥99%) were injected in their respective experiments by blowing heated (60°C) N_2 at 2 Lpm. Because of its low vapor pressure, hydroxybenzyl alcohol (HBA) (Sigma Aldrich) was injected in a slightly different manner. A known amount of HBA was dissolved in MilliQ water which was then atomized into the chamber. Similarly, ammonium sulfate ($(NH_4)_2SO_4$) (0.06 M) solution in MilliQ water was atomized to seed all yield experiments. The $(NH_4)_2SO_4$ particles were also dried and charge-conditioned with a TSI Model 3088 soft x-ray neutralizer prior to injection. Approximately 1×10^4 cm^{-3} of ammonium sulfate seed aerosol was used in all experiments. In all yield experiments reported in this chapter, NO (506.9 ppm ± 2%, Airgas Specialty Gases, Certified Standard) was diluted into the chamber. Experiments were conducted at ambient temperature (~ 291 K) and dry conditions (< 10%).

After all analytes were injected into the environmental chamber, data were collected for a ≥ 1 h background period to determine averaged initial VOC, NO, and seed aerosol mixing ratios. SOA yields were calculated as the amount of aerosol formed divided by the amount of reacted starting VOC (SOA Yield = $\frac{\Delta SOA}{\Delta VOC}$). A summary of experiments can be found in Table 3.1.

Expt. #	VOC	VOC Concentration (ppb)	[NO] (ppb)	H_2O_2 (ppb)
1	Benzyl alcohol	199	77	2,000
2	Benzyl alcohol	191	4.8	2,000
3	Benzyl alcohol	190	14	2,000
4	Benzyl alcohol	166	64	2,000
5	Benzyl alcohol	183	76	2,000
6	Benzyl alcohol	167	111	2,000
7	Benzyl alcohol	189	200	2,000
8	Benzyl alcohol	189	81	2,000
9	Benzyl alcohol	136	71	2,000
10	Benzyl alcohol	139	70	2,000
11	Benzyl alcohol	325	69	2,000
12	Benzyl alcohol	152	138	2,000
13	Hydroxybenzyl alcohol	191	159	2,000
14	Benzaldehyde	190	72	2,000

Table 3.1: SOA experiments conducted to quantify SOA yields and to analyze SOA chemical composition.

In-situ Measurements

A Teledyne Nitrogen Oxide Analyzer (Model T200) was used to measure the NO and NO_2 concentrations throughout the experiments. Ozone was measured with a Horiba Ambient Monitor. A CF_3O^- chemical ionization mass spectrometer (CIMS) with a Varian 1200 triple quadrupole mass analyzer was used to monitor VOC concentrations, including benzyl alcohol and HBA, and many of their subsequent oxidation products. The CIMS measured analytes at mass-to-charge ratios (mz) equal to the analyte atomic mass unit (amu) plus either the reagent ion cluster (CF_3O^-) or transfer ion (F^-) mass. The CIMS scanned for mz ratios between 50 and 330. The CF_3O^- CIMS is ideal for studying atmospherically relevant compounds because it is sensitive to a range of oxygenated compounds. It is not, however, sensitive to all compounds in the benzyl alcohol system, namely benzaldehyde, one of the main oxidation products. As such, gas chromatography with a flame ionization detect (GC-FID) was used to monitor the benzaldehyde concentration in Experiment 14.

Particle size and number were measured via a custom-built scanning mobility particle sizer (SMPS) with a 308100 TSI Differential Mobility Analyzer (DMA) and a TSI 3010 butanol condensation particle counter (CPC). Data inversion was performed using the method described elsewhere (Mai, 2018). Particle volume was

converted to mass using an average SOA density of 1.4 g cm^{-3}, based on past work (Kroll et al., 2006; Li et al., 2018). Measured aerosol were corrected for wall-loss was accounted for by fitting the background data using the eddy-diffusivity coefficient (k_e) and the mean electric field experienced within the chamber ($\bar{E}$) as parameters, as described in Charan, Huang, et al., 2019. Two treatments were considered: one where the proportionality factor, ω, was set to unity and another in which $\omega = 0$. In the $\omega = 0$ case, oxidation products with a sufficiently low vapor pressure to condense were assumed to do so only on suspended particles and not on particles that had deposited on the chamber walls (Weitkamp et al., 2007). When $\omega = 1$, on the other hand, condensable oxidation products and particles deposited on the chamber walls during the experiment were assumed to be in equilibrium with one another (Weitkamp et al., 2007).

Offline Analysis

For Experiments 2 – 12, the chemical composition of SOA was further analyzed using offline ultra-high performance liquid chromatography electrospray ionization quadruple time of flight mass spectrometry (UPLC/ESI-Q-ToFMS) hereforth referred to as UPLC-MS (Zhang et al., 2016). Post-oxidation samples were taken using 47 mm Pall Teflon filters, which were collected for ≥2 hours at 6.5 Lpm using an upstream activated carbon denuder. Additional Teflon filters were collected during photooxidation at 2 Lpm. This experimental set up is described by Kenseth et al., 2018. The SOA collected was extracted by placing each filter sample into 6 mL of milliQ water and agitating the samples on an orbital shaker for 1 h. In an effort to prevent on-filter chemistry from occurring, samples were stored at -14°C after initial collection and before extraction. Analysis using UPLC-MS was carried out in negative mode (where the parent molecule is observed at M-H) which is sensitive to the nitroaromatics formed in the aerosol-phase. The 12 min eluent program for UPLC-MS and MS/MS fragmentation analysis required 4 µL of sample with gradient eluents between a 0.1% formic acid/99.9% water solution and a 100% acetonitrile solution. The total flow rate was 0.3 mLpm, and masses were scanned from m/z = 40 to 1000. The method was similar to that in Kenseth et al., 2018. MassLynx software was used to analyze the resulting spectra, which calculates possible chemical formulas based on masses quantified during analysis. Mass assignments were limited to carbon-, oxygen-, and nitrogen-containing formulas as these were the only chemically viable formulas for benzyl alcohol oxidation chemistry. The structures assigned to chemical formulas from MassLynx analysis were based on

Compound	Polarizability	Dipole Moment
Benzyl alcohol	10.07	1.282
o-hydroxy benzyl alcohol	12.63	2.109
p-hydroxy benzyl alcohol	12.76	1.286

Table 3.2: Polarizabilities and dipole moments calculated for calibration purposes.

structures that corresponded to expected oxidation products and were confirmed based on MS/MS fragmentation analysis. Isomeric analysis was not conducted for these compounds, thus structures in Table 3.3 represent just one possible isomer. Several experiments with similar reaction conditions (Experiments 8 – 10) were analyzed to probe reproducibility of this technique. Reproducibility experiments showed consistent results.

Calibrations

Starting VOCs were calibrated to exact mixing ratios. Benzyl alcohol and HBA were calibrated to the CIMS and benzaldehyde was calibrated to the GC-FID. Benzyl alcohol and benzaldehyde were calibrated using a similar method. First, a known amount of the calibrant was injected into a 800 L Teflon "pillow" bag. The concentration in the pillow bag was measured using a Fourier transform infrared absorption (FTIR) spectrometer with a 19 cm pyrex cell with CaF_2 windows. The FTIR spectra were compared the FTIR spectra with the absorption cross sections from the Pacific Northwest National Laboratory (PNNL) database to calculate an absolute concentration. Multiple FTIR samples were taken until a consistent spectra signal was achieved. The calibrant in the pillow bag was then diluted to a concentration within the detection limit of the CIMS or GC-FID. and measured by the CIMS or GC-FID. The calibrant in the pillow bag was then diluted to a concentration within the detection limit of the CIMS or GC-FID. The calibrants were sampled for a sufficient amount of time to ensure a consistent signal was reached. Because HBA has a lower vapor pressure, calibrations were conducted differently by determining the ion–molecule collision rate relative to benzyl alcohol as described in Su et al., 1982. Polarizabilities and dipole moments for HBA and benzyl alcohol were calculated using quantum calculations described elsewhere (Garden et al., 2009). These values are reported in Table 3.2.

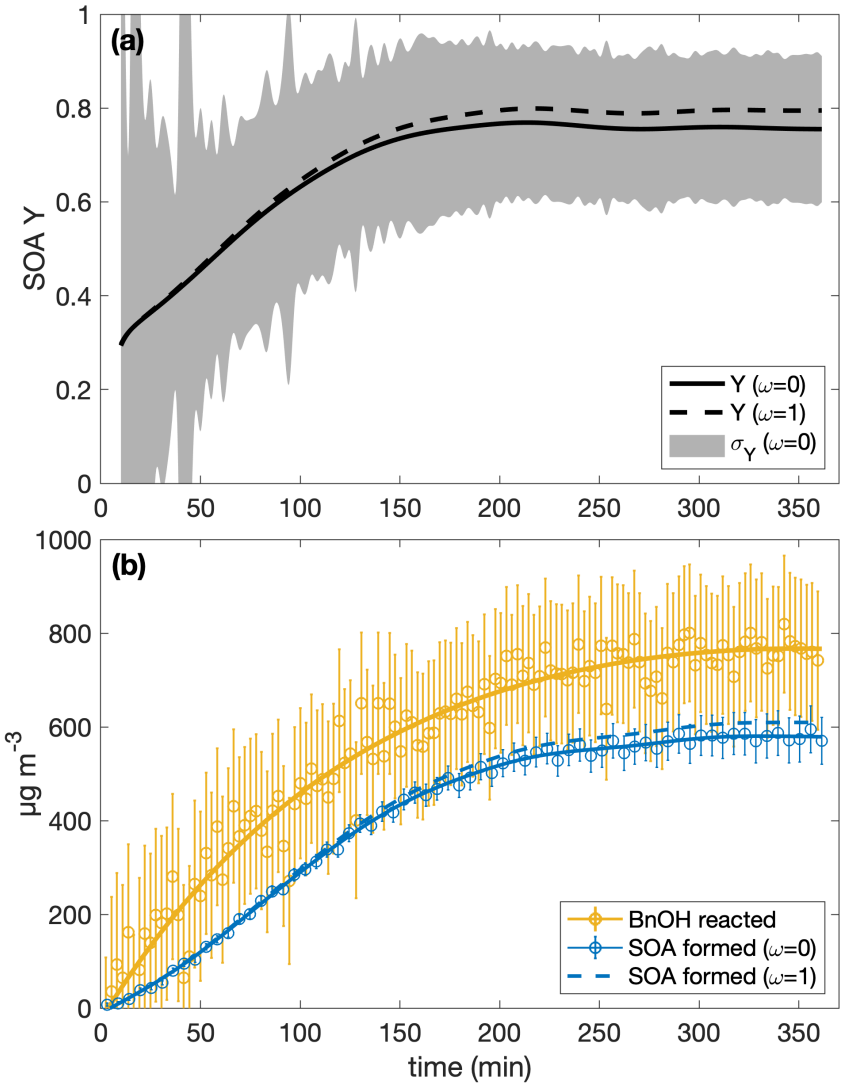

Figure 3.1: Yield of benzyl alcohol (a) calculated by dividing the amount of SOA formed by amount of benzyl alcohol reacted (b).

3.3 Results and Discussion

SOA Yields

The SOA yield of benzyl alcohol where [NO] = ~ 80 ppb (Experiment 1) is 0.76 ± 0.16 for the $\omega = 0$ case and 0.79 ± 0.16 for the $\omega = 1$ case (Figure 3.1). These values are considerably higher than the value used in McDonald et al., 2018, for example. To understand the high SOA yield of benzyl alcohol, we turn to the oxidation chemistry of benzyl alcohol explored in Chapter 2.

As detailed in Chapter 2, the primary oxidation products of benzyl alcohol are HBA and benzaldehyde. Because HBA has a much lower vapor pressure than benzaldehyde, HBA likely contributed more to SOA formation in benzyl alcohol oxidation

than benzaldehyde. This hypothesis was tested by conducting SOA experiments using HBA and benzaldehyde as the VOC precursors (Experiments 13 and 14). We estimate the relative contributions of HBA and benzaldehyde to benzyl alcohol SOA formation using these SOA yield experiments using HBA and benzaldehyde as the VOC precursors. Conditions for SOA experiments were selected to match those of the benzyl alcohol SOA yield experiments in Charan, Buenconsejo, et al., 2020 (Experiment 1).

Figure 3.1 shows results for SOA yield experiments using benzaldehyde and HBA. Note the OH exposures for benzaldehyde and HBA in these experiments were $\sim 2.8 \times 10^{10}$ molecule s cm^{-3} and $\sim 2.8 \times 10^{11}$ molecule s cm^{-3}, respectively, which corresponds to $\sim$ 52 min - 8.6 h of OH exposure on a typical Los Angeles summer day (Appendix 3.6) (Griffith et al., 2016). Both experiments were allowed to react for the same amount of time, $\sim$ 400 minutes, to compare to the SOA yield experiments conducted in Charan, Buenconsejo, et al., 2020. Therefore, the SOA yields of HBA and benzaldehyde are reported at t = 400 mins (SOA $Y_{400mins}$), rather than at an equilibrium point. In the upper bound, (ω = 1), SOA $Y_{400mins}$ of HBA is 1.2 ± 0.14 and in the lower bound (ω = 0), 0.97 ± 0.13. For benzaldehyde, we report an upper bound of SOA $Y_{400mins}$ 0.35 ± 0.039 and a lower bound of 0.28 ± 0.039. While comparing SOA $Y_{400mins}$ is helpful in determining which pathways (addition versus abstraction) contribute to the high SOA yield of benzyl alcohol, this value does not necessarily inform atmospherically relevant SOA yields of benzaldehyde and HBA as inputs for models because modeled reaction time and conditions may not exactly match experimental ones. Therefore, we report the parameterized fit of the SOA yields as a function of absorbing organic mass concentration (M).

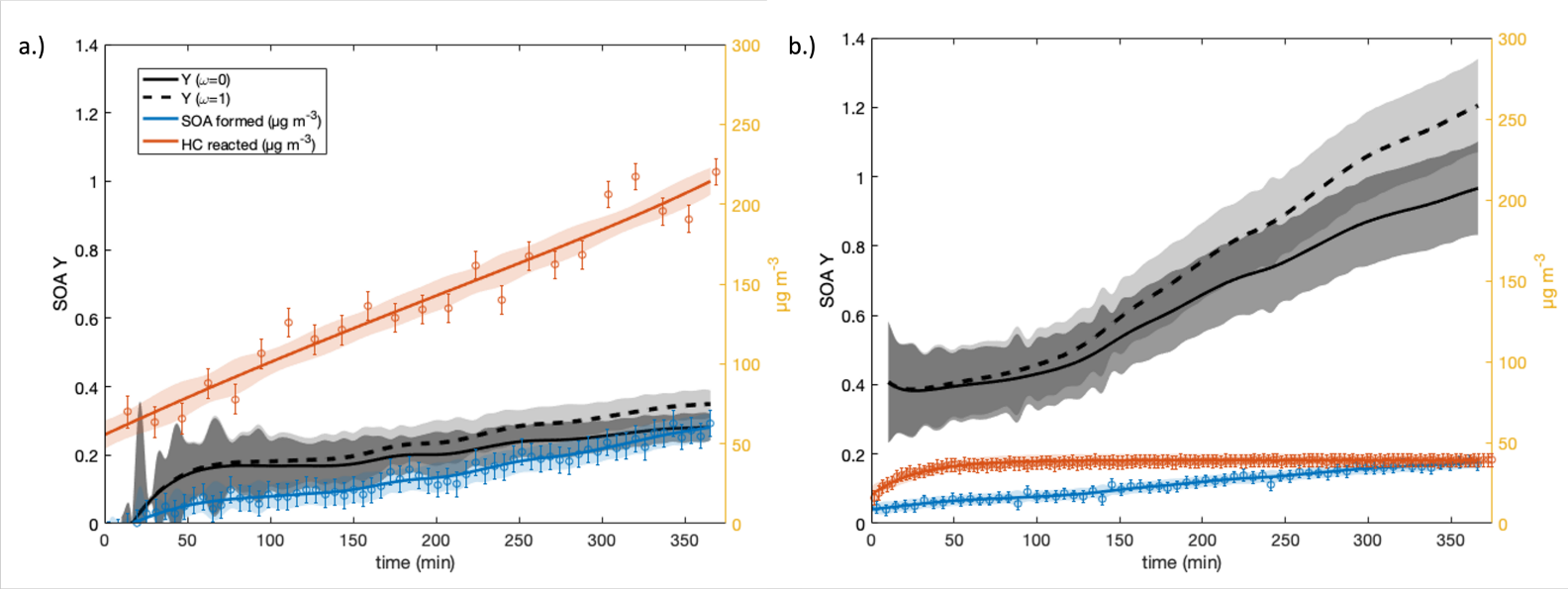

Figure 3.2: Wall-loss corrected SOA yields of (a) benzaldehyde and (b) HBA. Solid yields are calculated assuming $\omega = 0$. Dotted yields are calculated assuming ω equals unity. Red data are the amount of VOC precursor reacted in µg m^{-3}. Data displayed in blue are SOA formed in µg m^{-3}. Note that the first 10 minutes of SOA yield data are excluded because of the relatively high errors of the hydrocarbon reacted at the start of an experiment.

We follow a one-product parameterization method that follows the multiple paramterization described in Odum et al. (1996) where,

$$Y = M \times (\frac{\alpha K_{om}}{1 + K_{om} \times M}) \tag{3.1}$$

Here α, K_{om} is the partitioning coefficient and where α is a constant relating the total concentration of products formed with the amount of organic gas-phase mass reacted. The parameters in Equation 3.1 were chosen by minimizing the least square fit to the data (Appendix 3.5). Results for benzaldehyde SOA yield are graphed in Figure 3.3 ($\alpha = 0.34 \pm 0.013$ and $K_{om} = (9.4 \pm 1.2) \times 10^{-3}$). For HBA, this approach becomes more complicated. The Odum et al. approach uses the steady state approximation (SSA) which states that the derivative of the concentration of an intermediate species appears to be zero. In other words, we assumed an approximately steady state of first-generation oxidation products which are reacting at roughly the same rate as their formation. The rates of reaction of HBA and subsequent oxidation products were likely unequal because the HBA reacts away early in the experiment; therefore, the SSA was not a sufficient approximation and so, we did not use the Odum et al. fitting for HBA.

At t = 400 mins, unreacted benzaldehyde remained in the chamber whereas HBA reacted within the t < 1 h of the experiment. This may indicate that the SOA formed in the benzaldehyde experiments is from the very rapid chemistry of subsequent generation oxidation products, as is the case with toluene. In the HBA experiments, most of the SOA is likely also generated from the oxidation of later-generation products.

Because HBA had a much larger SOA yield than benzaldehyde, HBA likely contributed most significantly to the large measured SOA yield of benzyl alcohol in our experiments. The rapid reaction of HBA likely leads to other products with increasing OH kinetics. In aromatic oxidation chemistry, addition of electron-donating groups (such as OH) lowers the barrier of reaction for additional OH chemistry (Calvert et al., 2002). With benzene, adding electron-donating substituent groups can increase reactivity with OH by $\sim 4 - 8$x. In the benzyl alcohol system, after every subsequent reaction with the OH radical, we anticipate the kinetics of HBA quickly lead to low-volatility, highly-oxygenated products that readily partition into aerosol.

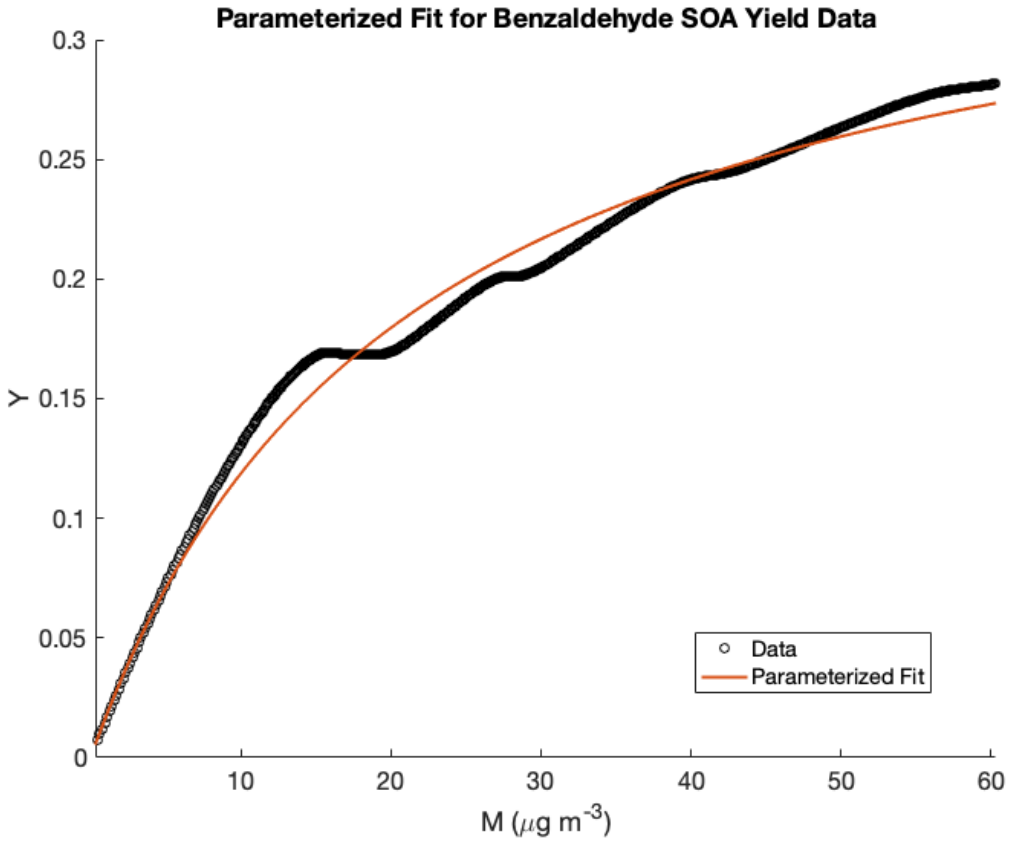

Figure 3.3: Parameterization of SOA yield data as a function of organic mass reacted. Because SOA yields did not stabilize in these experiments, parameterization can be useful in contextualizing SOA yields under atmospherically relevant conditions.

As described in Chapter 2, the branching ratios of HBA and benzalehdye appear to be invariable with changing NO mixing ratios. The SOA yields of benzyl alcohol, however, do appear to vary slightly with NO mixing ratio (Figure 3.4). Because the gas-phase branching ratios are not necessarily dependent on [NO], we do not anticipate that the variations of benzyl alcohol SOA yields are due to changes in increased or decreased access to primary oxidative pathways. Thus, differences in SOA yields may be due to the formation of products formed only under higher NO mixing ratios: organonitrates (RNO_2). The following section details results on the chemical composition of the aerosol formed during benzyl alcohol experiments that corroborate this hypothesis.

SOA Chemical Composition

The UPLC-MS analysis found a high prevalence of $RONO_2$, specifically nitroaromatics (Table 3.3). This indicates that many of the low-volatility products that

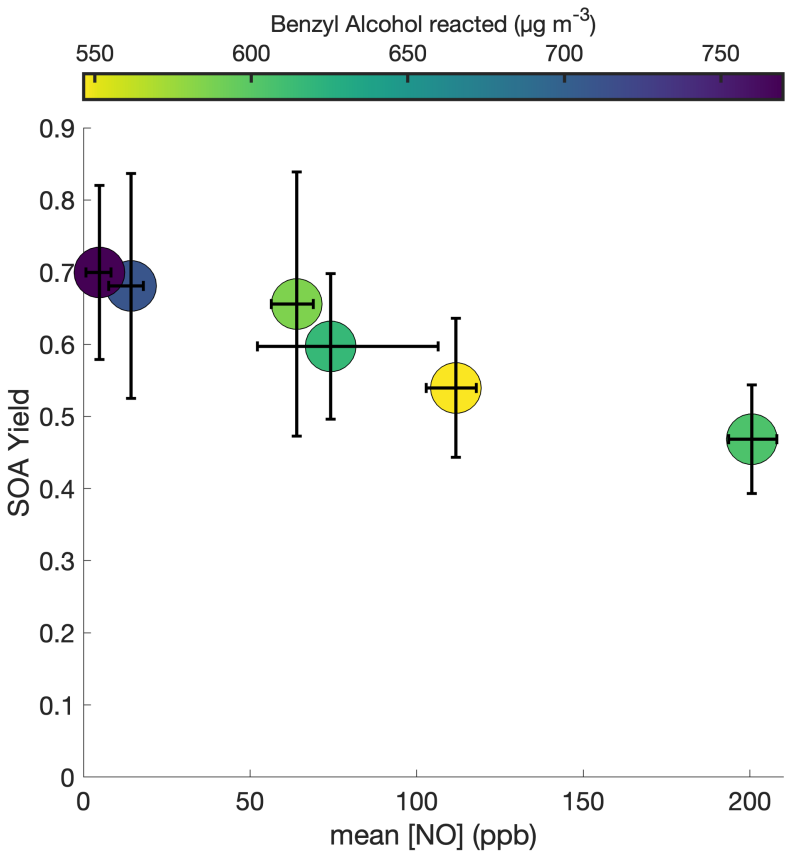

Figure 3.4: The SOA yields of benzyl alcohol vary slightly with varying constant NO mixing ratios (Experiments 2 – 7).

condense into the aerosol phase retain their aromatic structure. Many of these aerosol-phase products were C7 compounds though several C6 compounds were also observed. This is congruent with the gas-phase chemical mechanism results discussed in Ch 2., which indicate that the methanol functional group can be lost to form C6 products. One particularly prominent C6 product observed via UPLC-MS was nitrocatechol.

It is possible, however, that there are other organic compounds present in the SOA, including non-ring-retaining compounds, that are not sensitive to UPLC-MS detection. The prevalence of nitroaromatics may be a result of the UPLC analysis method that is particularly sensitive to nitroaromatics: the UPLC-MS exhibits different sensitivities to compounds depending on the polarizability of the compound as well as its ability to ionize. It is likely that the UPLC-MS is quite sensitive to the nitroaromatics reported in this work as compared to other compounds. The detection of aerosol-phase compounds via UPLC-MS is limited to compounds that are water soluble, are able to elute from the chromatographic column, are detectable

Retention Time (RT)	Mass (mz)	Error (mDa)	Molecular Formula	Representative Isomer
3.484, 5.384	138.0147	-3.9, -4.4	$C_6H_5NO_3$	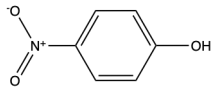
3.857	137.0195	-3.9, -4.4	$C_7H_6O_3$	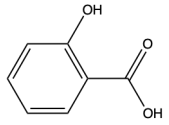
3.956, 4.485, 4.653	170.0047/2/5	-4.4	$C_6H_5NO_5$	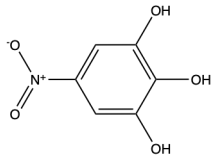
4.165, 4.180	184.0199/7	-4.7, -5.0	$C_7H_7NO_5$	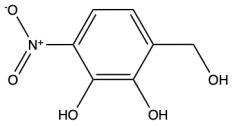
4.279	148.0352	-	unassigned	
4.348	121.0245	-4.5	$C_7H_6O_2$	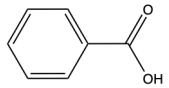
4.561	168.0250	-4.7	$C_7H_7NO_4$	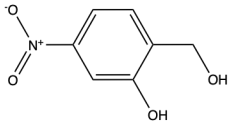
4.759	154.0096	-4.4	$C_6H_5NO_4$	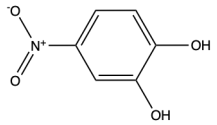
4.820, 5.079, 5.346	182.0047	-3.9	$C_7H_5NO_5$	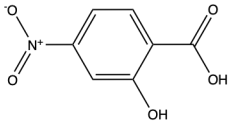
5.673	166.0097	-4.3	$C_7H_5NO_4$	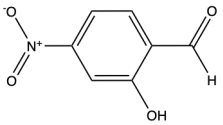
5.719	198.9991	-4.2	$C_6H_4N_2O_6$	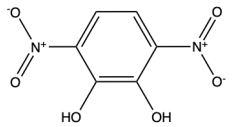

Table 3.3: Peak assignments for UPLC-MS analysis.

in negative ion mode, and lie within the detection limits of the instrument (Surratt et al., 2008). An additional limitation of this method is the possibility of filter chemistry post-collection. For example, there may have been aqueous-phase chemistry during the extraction phase. Though filters were stored at low temperatures, on-filter chemistry may also have occurred. This could alter the molecular weight of the original compounds collected in the particle phase (Zhang et al., 2016).

Regardless, the importance of $RONO_2$ to forming aerosol in high NO conditions is clear. This is congruent with past work on other aromatic systems including toluene.

3.4 Conclusion

This chapter included work examining the formation of SOA from benzyl alcohol oxidation by OH. Benzyl alcohol reacts with OH to primarily form two first-generation products. HBA and benzaldehyde. Aerosol yield studies using HBA and benzaldehyde as the precursors suggested that the HBA pathway is important to the high SOA yields observed in benzyl alcohol oxidation. HBA is quickly oxidized by OH to form low-volatility products which rapidly partition to the particle phase, thus contributing to the high SOA yield of benzyl alcohol.

The chemical composition of the aerosol formed by benzyl alcohol oxidation was also analyzed. C7 and C6 aromatic compounds were found in the particle phase, congruent with gas-phase conclusions outlined in Chapter 2.

Though VCPs have been identified as increasingly important to SOA formation, key VCP-derived SOA remain uncharacterized. This work can be used to consider other aromatic SOA potential and chemical composition.

APPENDIX

3.5 Parameterization of SOA Yields

We report the results of the parameters from the least square fit for benzaldehyde derived SOA. For Eq. 6, $\alpha = 0.34 \pm 0.013$ and $K_{om} = (9.4 \pm 1.2) \times 10^{-3}$. The fit has an r-squared value of 0.90.

3.6 OH Exposure

[OH] was calculated for SOA yield experiments using the kinetic equation:

$$\frac{d[\text{reagent}]}{dt} = -k_{OH}[OH][\text{reagent}]. \tag{3.2}$$

Here, $\frac{d[\text{reagent}]}{dt}$ was determined by finding the slope of the starting reagent against time. For benzaldehyde, the slope over the entire experiment was used. For HBA, the slope for the first 15 min was used to determine [OH] for the experiment.

3.7 GC-FID Operation

To quantify benzaldehyde a GC-FID was used with a DB-5 column. The GC-FID was run from 40°C to 250° C with a ramp rate of 50°C/min.

References

Calvert, Jack G., Atkinson, Roger, Becker, Karl H., Kamens, Richard M., John H. Seinfeld, Wallington, Timothy J., and Yarwood, Greg (2002). *The mechanism of atmospheric oxidation of aromatic hydrocarbons*. New York, New York: Oxford University Press.

Charan, Sophia M., Reina S. Buenconsejo, and John H. Seinfeld (Nov. 2020). "Secondary organic aerosol yields from the oxidation of benzyl alcohol". en. In: *Atmospheric Chemistry and Physics* 20.21, pp. 13167–13190. ISSN: 1680-7324. DOI: 10.5194/acp-20-13167-2020. URL: https://acp.copernicus.org/articles/20/13167/2020/ (visited on 10/26/2021).

Charan, Sophia M., Yuanlong Huang, and John H. Seinfeld (Dec. 2019). "Computational simulation of secondary organic aerosol formation in laboratory chambers". en. In: *Chemical Reviews* 119.23, pp. 11912–11944. ISSN: 0009-2665, 1520-6890. DOI: 10.1021/acs.chemrev.9b00358. URL: https://pubs.acs.org/doi/abs/10.1021/acs.chemrev.9b00358 (visited on 11/30/2020).

Finlayson-Pitts, Barbara and Pitts, James N. Jr. (1986). *Atmospheric chemistry: fundamentals and experimental techniques*. United States: Wiley-Interscience. ISBN: 0-471-88227-5.

Garden, Anna L., Fabien Paulot, John D. Crounse, Isobel J. Maxwell-Cameron, Paul O. Wennberg, and Henrik G. Kjaergaard (May 2009). "Calculation of conformationally weighted dipole moments useful in ion–molecule collision rate estimates". en. In: *Chemical Physics Letters* 474.1-3, pp. 45–50. ISSN: 00092614. DOI: 10.1016/j.cplett.2009.04.038. URL: https://linkinghub.elsevier.com/retrieve/pii/S0009261409004679 (visited on 03/13/2024).

Griffith, S. M., R. F. Hansen, S. Dusanter, V. Michoud, J. B. Gilman, W. C. Kuster, P. R. Veres, M. Graus, J. A. Gouw, J. Roberts, C. Young, R. Washenfelder, S. S. Brown, R. Thalman, E. Waxman, R. Volkamer, C. Tsai, J. Stutz, J. H. Flynn, N. Grossberg, B. Lefer, S. L. Alvarez, B. Rappenglueck, L. H. Mielke, H. D. Osthoff, and P. S. Stevens (Apr. 2016). "Measurements of hydroxyl and hydroperoxy radicals during CalNex-LA: Model comparisons and radical budgets". en. In: *Journal of Geophysical Research: Atmospheres* 121.8, pp. 4211–4232. ISSN: 2169-897X, 2169-8996. DOI: 10.1002/2015JD024358. URL: https://onlinelibrary.wiley.com/doi/10.1002/2015JD024358 (visited on 08/30/2023).

Henze, D.K., J.H. Seinfeld, N.L. Ng, and J.H. Kroll (2008). "Global modeling of secondary organic aerosol formation from aromatic hydrocarbons: high- vs. low-yield pathways". en. In: *Atmospheric Chemistry and Physics*.

Kenseth, Christopher M., Yuanlong Huang, Ran Zhao, Nathan F. Dalleska, J. Caleb Hethcox, Brian M. Stoltz, and John H. Seinfeld (2018). "Synergistic O3 + OH oxidation pathway to extremely low-volatility dimers revealed in beta-pinene secondary organic aerosol". In: *Proceedings of the National Academy of Sciences*

115.33, pp. 8301–8306. ISSN: 0027-8424. DOI: 10.1073/pnas.1804671115. URL: https://www.pnas.org/content/115/33/8301.

Kroll, Jesse H., Nga L. Ng, Shane M. Murphy, Richard C. Flagan, and John H. Seinfeld (Mar. 2006). "Secondary organic aerosol formation from isoprene photooxidation". en. In: *Environmental Science & Technology* 40.6, pp. 1869–1877. ISSN: 0013-936X, 1520-5851. DOI: 10.1021/es0524301. URL: https://pubs.acs.org/doi/10.1021/es0524301 (visited on 04/09/2020).

Li, Lijie and David R. Cocker (May 2018). "Molecular structure impacts on secondary organic aerosol formation from glycol ethers". en. In: *Atmospheric Environment* 180, pp. 206–215. ISSN: 13522310. DOI: 10.1016/j.atmosenv.2017.12.025. URL: https://linkinghub.elsevier.com/retrieve/pii/S1352231017308610 (visited on 01/26/2019).

Mai, Huajun (May 2018). "Scanning Electrical Mobility Methods for Aerosol Characterization". en. PhD thesis. California Institute of Technology. URL: 10.7907/9D4H-QS44.

McDonald, Brian C., Joost A. de Gouw, Jessica B. Gilman, Shantanu H. Jathar, Ali Akherati, Christopher D. Cappa, Jose L. Jimenez, Julia Lee-Taylor, Patrick L. Hayes, Stuart A. McKeen, Yu Yan Cui, Si-Wan Kim, Drew R. Gentner, Gabriel Isaacman-VanWertz, Allen H. Goldstein, Robert A. Harley, Gregory J. Frost, James M. Roberts, Thomas B. Ryerson, and Michael Trainer (Feb. 2018). "Volatile chemical products emerging as largest petrochemical source of urban organic emissions". en. In: *Science* 359.6377, pp. 760–764. ISSN: 0036-8075, 1095-9203. DOI: 10.1126/science.aaq0524. URL: http://www.sciencemag.org/lookup/doi/10.1126/science.aaq0524 (visited on 10/12/2018).

Ng, N.L., J.H. Kroll, A.W.H. Chan, P.S. Chhabra, R.C. Flagan, and J.H. Seinfeld (2007). "Secondary organic aerosol formation from m-xylene, toluene, and benzene". en. In: *Atmospheric Chemistry and Physics*, p. 14.

Pennington, Elyse A., Karl M. Seltzer, Benjamin N. Murphy, Momei Qin, John H. Seinfeld, and Havala O. T. Pye (Dec. 2021). "Modeling secondary organic aerosol formation from volatile chemical products". en. In: *Atmospheric Chemistry and Physics* 21.24, pp. 18247–18261. ISSN: 1680-7324. DOI: 10.5194/acp-21-18247-2021. URL: https://acp.copernicus.org/articles/21/18247/2021/ (visited on 05/19/2022).

Su, Timothy and Walter J. Chesnavich (May 1982). "Parametrization of the ion-polar molecule collision rate constant by trajectory calculations". en. In: *The Journal of Chemical Physics* 76.10, pp. 5183–5185. ISSN: 0021-9606, 1089-7690. DOI: 10.1063/1.442828. URL: https://pubs.aip.org/jcp/article/76/10/5183/89898/Parametrization-of-the-ion-polar-molecule (visited on 03/13/2024).

Surratt, Jason D., Yadian Gómez-González, Arthur W. H. Chan, Reinhilde Vermeylen, Mona Shahgholi, Tadeusz E. Kleindienst, Edward O. Edney, John H. Offenberg, Michael Lewandowski, Mohammed Jaoui, Willy Maenhaut, Magda Claeys, Richard C. Flagan, and John H. Seinfeld (Sept. 2008). "Organosulfate Formation in Biogenic Secondary Organic Aerosol". en. In: *The Journal of Physical Chemistry A* 112.36, pp. 8345–8378. ISSN: 1089-5639, 1520-5215. DOI: 10.1021/jp802310p. URL: https://pubs.acs.org/doi/10.1021/jp802310p (visited on 12/13/2022).

Vereecken, Luc (Jan. 2019). "Reaction Mechanisms for the Atmospheric Oxidation of Monocyclic Aromatic Compounds". en. In: *Advances in Atmospheric Chemistry*. World Scientific, pp. 377–527. ISBN: 978-981-327-182-1 978-981-327-183-8. DOI: 10.1142/9789813271838_0006. URL: https://www.worldscientific.com/doi/abs/10.1142/9789813271838_0006 (visited on 11/14/2019).

Wang, Liming (May 2015). "The Atmospheric Oxidation Mechanism of Benzyl Alcohol Initiated by OH Radicals: The Addition Channels". en. In: *ChemPhysChem* 16.7, pp. 1542–1550. ISSN: 14394235. DOI: 10.1002/cphc.201500012. URL: http://doi.wiley.com/10.1002/cphc.201500012 (visited on 06/03/2019).

Weitkamp, Emily A., Amy M. Sage, Jeffrey R. Pierce, Neil M. Donahue, and Allen L. Robinson (Oct. 2007). "Organic Aerosol Formation from Photochemical Oxidation of Diesel Exhaust in a Smog Chamber". en. In: *Environmental Science & Technology* 41.20, pp. 6969–6975. ISSN: 0013-936X, 1520-5851. DOI: 10.1021/es070193r. URL: https://pubs.acs.org/doi/10.1021/es070193r (visited on 02/08/2022).

Zafonte, Leo, Paul L. Rieger, and John R. Holmes (May 1977). "Nitrogen dioxide photolysis in the Los Angeles atmosphere". en. In: *Environmental Science & Technology* 11.5, pp. 483–487. ISSN: 0013-936X, 1520-5851. DOI: 10.1021/es60128a006. URL: https://pubs.acs.org/doi/abs/10.1021/es60128a006 (visited on 06/20/2023).

Zhang, X., N.F. Dalleska, D.D. Huang, K.H. Bates, A. Sorooshian, R.C. Flagan, and J.H. Seinfeld (Apr. 2016). "Time-resolved molecular characterization of organic aerosols by PILS + UPLC/ESI-Q-TOFMS". en. In: *Atmospheric Environment* 130, pp. 180–189. ISSN: 13522310. DOI: 10.1016/j.atmosenv.2015.08.049. URL: https://linkinghub.elsevier.com/retrieve/pii/S1352231015302946 (visited on 11/06/2019).

Chapter 4

CHEMISTRY AND SOA FORMATION FROM GLYCOL ETHERS

4.1 Abstract

This chapter examines the SOA formation from 2-ethoxyethanol (2-EE), a VCP used as an industrial solvent, cleaning supplies, and paints. Using a 19 m^3 environmental smog chamber, SOA yields of 2-EE is probed over a range of NO and HO_2 mixing ratios to better understand SOA formation as a function of peroxy (RO_2) bimolecular lifetime. In low-NO_x conditions, the unimolecular hydrogen shift reaction to the 2-EE peroxy radicals has been shown to be important, making this autoxidation competitive with bimolecular pathways. The autoxidation pathway effectively leads to the formation of high O:C ratio oxidation products and may also lead to the formation of an epoxy radical; compounds that will readily partition to SOA. This work shows that SOA yields increase as the 2-EE RO_2 bimolecular lifetime increases. Thus it appears the autoxidation pathway is effective at forming higher yields of SOA than under conditions previously studied. This work is relevant to urban environments like the Los Angeles Basin where NO_x levels and other vehicular emissions continue to decrease but where VCPs are continuing to play an important role in air quality.

4.2 Introduction

Glycol ethers are widely used in volatile chemical products (VCPs) such as cleaning products, cosmetics, and soaps (Singer et al., 2006; (EPA), 2016). Glycol ethers are also prevalent in some biodiesels, making up as much as $\sim$ 9% of the VOC emissions of one blend (Lopes et al., 2014). Acute and chronic exposure to glycol ethers can lead to human health effects such as narcosis, liver and kidney damage, and anemia ((EPA), 2016). Emissions of glycol ethers are also significant to the outdoor atmosphere, with one study estimating 13.44 tons of glycol ether emitted per day in the state of California (Cocker et al., 2014).

Given the prevalence of glycol ethers in both indoor and outdoor settings, it is important to study and characterize its reactivity. In the daytime, ethoxyethanol (2-EE) is primarily lost to the OH radical which reacts at room temperature at a rate of $(1.94 \pm 0.2) \times 10^{-11}$ cm^3 $molecule^{-1}$ s^{-1}, respectively (Stemmler, Kinnison, et al., 1996; Aschmann et al., 1998). This is in good agreement with a more recent

study of 2-EE which measured $k_{OH+2EE} = (2.17 \pm 0.11) \times 10^{-11}$ cm^3 molecule^{-1} s^{-1} (Colmenar et al., 2020). The kinetics of 2-EE with Cl, OH, and NO_3 are much slower, at rates of $(2.02 \pm 0.19) \times 10^{-10}$, $(2.7 \pm 0.11) \times 10^{-11}$, and $(4.80 \pm 0.48) \times 10^{-15}$ cm^3 mol^{-1} s^{-1}, respectively (Colmenar et al., 2020). Past work has also identified gas-phase products.

In laboratory experiments, Stemmler et al. (1996) identified ethyl formate, ethoxyacetaldehyde, and ethylene glycol monoformate as primary oxidation products of 2-EE + OH (Stemmler, Mengon, et al., 1997). Similar products were identified in the 2-EE study by Colmenar et al. (2020). Note that the products identified in the Stemmler et al. study have homologues with 2-butoxyethanol, indicating 2-EE may be a good proxy for representing other glycol ethers.

The secondary organic aerosol (SOA) formation from 2-EE is less well-studied. One previous study looked at a suite of glycol ethers under NO-only, H_2O_2-only, and H_2O_2 + NO conditions (Li et al., 2018). This studied hypothesized that the OH functional group in ethers played an important role in the formation of SOA. Quantification and additional characterization of SOA formed by 2-EE, thus, is still needed. It is important to study SOA formation under different NO_x conditions, particularly as U.S. and other urban areas around the world are experiencing a shift in average NO mixing ratios which can lead to different chemical pathways. Autoxidation has been identified as one such important chemical pathway that can typically become significant when [NO] $<$ 100 ppt (Crounse, Nielsen, et al., 2013). Until recently autoxidation—where intermolecular and intramolecular H-shifts occur in peroxy radicals—had not been considered substantially in atmospheric contexts (Crounse, Nielsen, et al., 2013).

Recently, 2-EE was shown to readily autoxidize under conditions corresponding to $\sim$ 500 ppt NO and under typical ambient conditions(Yu et al., 2023). This work showed that several of the H-shifts that occur when 2-EE forms its peroxy radical proceed as fast as 0.1 s^{-1} when bimolecular lifetimes are $\leq$ 10 s (Yu et al., 2023). The autoxidation products of 2-EE form high O:C ratio products that may lead to SOA, and may even form an epoxide; epoxides have been show to be significant in the formation of SOA in other systems (Chan et al., 2010; Nguyen et al., 2014; Surratt et al., 2010).

Autoxidation was first seriously considered in atmospheric contexts in Crounse et al. (2013). The reaction involves a unimolcular H-shift (usually 1,4 H-shift, 1,5 H-shift, or 1,6 H-shift) that occurs for some RO_2 intermediates (Figure 4.1). When

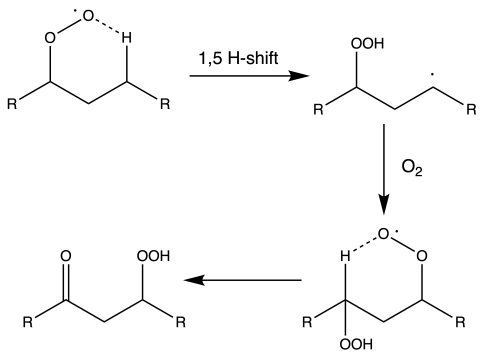

Figure 4.1: Autoxidation typically occurs when peroxy radical intermediate isomerizes an H-shift. This mechanism efficiently results in highly functionalized compounds.

this isomerization occurs, it can be an efficient way to rapidly form high O:C, low volatility products that can partition to SOA (Crounse, Knap, et al., 2012; Xu et al., 2020). This chemistry is increasingly germane as NO_x levels in major urban centers continue to decrease (Parker et al., 2020; Simon et al., 2015; Praske et al., 2018). Autoxidation can occur in most urban areas in the U.S. where [NO] is $0.1 - 10$ ppb (Crounse, Knap, et al., 2012). While "high NO" conditions are usually considered for integration into models, they may not accurately represent the NO_x mixing ratios in most American urban centers.

In this study we draw on the previously studied chemistry of 2-EE to investigate the SOA yields of of 2-EE. We quantified SOA yields across different NO mixing ratios and as a function of peroxy radial biomolecular lifetime. As described in Yu et al. (2023), when the peroxy radical bimolecular lifetime, τ_{RO2}, exceeds 10 s autoxidation accounts for $\sim$ 30% of the reactive RO_2 pathway (Yu et al., 2023). We hypothesize based of this previous work, that for similar bimolecular lifetimes, SOA formation from 2-EE will be more significant.

4.3 Methodology

Chamber Experiments

All experiments were conducted in the Caltech Environmental 19 m^3 FEP Teflon Chamber. Prior to each experiment, the chamber was continuously flushed for a minimum of 24 h. All experiments were run under dry conditions (RH $<$ 10%). Slyvania 350 nm (40 W) lights were used for oxidation. The lights were arranged with 16 lights in a panel and four panels lining either side of the chamber wall enclosure. Hydrogen peroxide (H_2O_2) was used as the oxidant source. Air was blown over aliquots of H_2O_2 warmed in a $\sim$ 42°C water bath. In all experiments

$\sim$ 2 ppm of H_2O_2 was used. All experiments were seeded using ammonium sulfate ($(NH_4)_2SO_4$). Seed aerosol was injected into the chamber by bubbling purified air through an aqueous (MilliQ) solution of $(NH_4)_2SO_4$ (0.06 M). Particles were dried and their charge was stripped using a soft X-ray neutralizer (TSI Model 3088).

NO (506.2 ppm ±2%, Airgas) was injected into the chamber for a set amount of time to achieve the desired mixing ratio. Adequate NO was injected such that there was always NO remaining at the end of the experiment. To adjust the HO_2 mixing ratios and thus τ_{RO2}, methanol (Sigma-Aldrich, > 99.9%) was used. Methanol forms HO_2 via the reaction:

$$CH_3OH + OH \xrightarrow{O_2} HO_2 + HCHO + H_2O. \tag{4.1}$$

While H_2O_2 also generates some amount of HO_2:

$$H_2O_2 \xrightarrow{h\nu} 2\,OH. \tag{4.2}$$

$$OH + H_2O_2 \longrightarrow HO_2 + H_2O. \tag{4.3}$$

The formation of HO_2 is dominated by the methanol pathway (Eq. 4.1). The amount of methanol injected was always much larger than the amount of VOC in order to constrain HO_2 mixing ratios and to minimize $RO_2 + RO_2$ chemistry. An ethylene glycol (Sigma-Aldrich, 99.8%) tracer was used as a proxy for determining amount of glycol ether reacted (see Gas-Phase Instrumentation for additional details). Ethylene glycol works well as a tracer because it has similar kinetics to that of 2-EE and because its oxidation products do not partition into the aerosol phase and so have minimal interference with quantifying SOA yield. The mixing ratio of OH over time was inferred by using the rate coefficient of ethylene glycol + OH, $(1.47 \pm 0.26) \times 10^{-11}$ cm^{-3} mol^{-1} s^{-1} (Aschmann et al., 1998). and by monitoring the reaction of ethylene glycol and formation of its primary oxidation product, glycoaldehyde:

$$HOCH_2CH_2OH \xrightarrow[O_2]{OH} HOCH_2CHO + H_2O + HO_2. \tag{4.4}$$

We assumed the k_{OH} of 2-EE to be $(1.94 \pm 0.2) \times 10^{-11}$ cm^3 $molecule^{-1}$ s^{-1} (Stemmler, Kinnison, et al., 1996; Aschmann et al., 1998). Using the inferred OH mixing ratio and the kinetic rate constants, Δ2-EE was calculated. A summary of experiments can be found in Table 4.1.

Experiment ID	VOC (ppb)	MeOH (ppm)	NO (ppb)	Lights	Temp (°C)
EE1	Ethoxyethanol (500)	0	0	100%	23
EE2	Ethoxyethanol (500)	45	0	100%	37
EE3	Ethoxyethanol (500)	45	0	33%	23
EE4	Ethoxyethanol (500)	45	0	100%	23
EE5	Ethoxyethanol (500)	0	1,000	100%	23

Table 4.1: Summary of experiments analyzed for this paper.

Instrumentation

Gas-Phase

A CF_3O^- chemical ionization mass spectrometer (CIMS) was employed to monitor gas-phase analytes. The CIMS uses a Varian 1200 triple quadrupole mass analyzer to scan through masses from 50 to 350 amu. The masses are measured as a sum of the analyte mass and the reagent ion (either CF_3O^- or F^-). For further information on the selective chemistry with the CIMS reagent ions, see Crounse et al. 2006 (Crounse, McKinney, et al., 2006). While the CIMS is sensitive to quantifying the initial mixing ratios of both 2-BE and 2-EE, oxidation products in both systems correspond with the masses of the starting analytes thus complicating quantification of 2-EE reacted. Therefore, ethylene glycol was used as a tracer as detailed in the Chamber Experiments section. Gas-phase analytes were normalized using the water (104 amu), the reagent ion (84 amu), and H_2O_2 (119 amu).

A Fourier transform infrared (FTIR) spectrometer with a 19 cm path length was used to calibrate the CIMS sensitivity to 2-EE and ethylene glycol. For calibrations, ppm-levels of the analytes were filled into an evacuated 0.5 L rounded bulb. The absolute concentration of the bulbs were calculated by comparing its measured FTIR spectrum to absorption cross sections from reference spectra provided by the Pacific Northwest National Laboratory (PNNL) database.

Ozone produced during the high NO experiments was monitored using a Horiba ambient monitor. NO and NO_2 mixing ratios were measured using a Model T200 Teledyne nitrogen oxide analyzer. Humidity and temperature were monitored via a Vaisala HMM211 probe.

Particle-Phase

Aerosol number and size distribution were measured using a custom-built scanning mobility particle sizer (SMPS) which scanned from 15 to 9875 V. This SMPS is

equipped with a TSI 3010 condensation particle counter (CPC) that use butanol and a TSI 3081 differential mobility analyzer (DMA). Aerosol sample is sent through an X-ray charge conditioner to give a known charge distribution.

SOA Yield and Bimolecular Lifetime Calculations

The SOA yields (SOA Y) were calculated by:

$$\text{SOA Y} = \frac{\Delta\text{SOA}_{\text{corrected}}}{\Delta\text{HC}} \tag{4.5}$$

Where $\Delta\text{SOA}_{\text{corrected}}$ refers to the wall-loss corrected SOA formed and ΔHC corresponds to the amount of 2-EE reacted. The Teflon chamber hangs suspended within a rigid enclosure. The enclosure prevents people and objects from inadvertently generating charge on the chamber (Charan, Kong, et al., 2018). Because the chambers are run in batch mode, the volume of the chambers decreases over time, though for most experiments the volume change is $< 20\%$, minimizing the amount the chamber walls touch each other or the enclosure. Experiment EE3, the experiment was run for $\sim$ 20 h because fewer lights were used for oxidation and had a change volume of $\sim 30\%$. Despite the relative isolation of the Environmental Chamber, there is still particle loss to the walls. This wall loss was determined by fitting 1 h data collected after all injections were completed and prior the irradiation period (henceforth referred to as the "background period"). The data were fit using two parameters, the eddy-diffusivity coefficient (k_e) and the mean electric field of the chamber ($\bar{E}$) (Charan, Huang, et al., 2019; Charan, Buenconsejo, et al., 2020). Because the chamber was typically undisturbed, $\bar{E} = 0$, however k_e varied from $\sim 0.01 - -0.2\ \text{s}^{-1}$. The minimization fit performed over the background period was then used to correct the remaining data.

SOA Y reported were compared to τ_{RO2} which was calculated by:

$$\tau_{\text{bimolecular}} = \frac{1}{k_{\text{RO2+NO}}[\text{NO}] + k_{\text{RO2+HO2}}[\text{HO}_2]}. \tag{4.6}$$

The k_{RO_2+NO} and $k_{RO_2+HO_2}$ values were used from literature values or from the Master Chemical Mechanism (MCM v3.3.1) (Jenkin et al., 1997; Saunders et al., 2003; Calvert et al., 2011). For reactions where NO was not added, [NO] = 0 was assumed. For reactions where methanol was added, $[HO_2]$ was calculated using methods described in Appendix 4.5.

Experiment	τ_{RO_2} (s)	SOA Y
EE1	1	13%
EE2	20 (high temp)	14%
EE3	20	22%
EE4	7	14%
EE5	0.005	4.5%

Table 4.2: Results of ethoxyethanol experiments.

4.4 Results and Discussion

SOA yields of ethoxyethanol range from $22 - 4.5\%$. These values correlate well with peroxy radical bimolecular lifetime τ_{RO_2} (Table 4.2).

Four major pathways exist for RO_2: NO, RO_2, HO_2, and unimolecular reaction. The NO pathway primarily leads primarily to alkoxy radical formation and nitrates ($RONO_2$); the $RO_2 \cdot RO_2$ self reaction leads to alkoxy radical formation and hydroxy terminal groups; reaction with HO_2 can often lead to carbonyl, hydroxy, and hydroperoxy functional groups; the unimolecular pathway, as discussed previously, can lead to high O:C ratio products including those with carbonyl and hydroperoxy groups. Whether or not a peroxy radical is able to proceed down any of these four chemical pathway depends on τ_{RO_2}. When ambient NO levels are ≤ 100 ppt, peroxy radical lifetimes are sufficiently long enough ($10 - 100$ s) for autoxidation to be competitive with HO_2, NO, and RO_2 reaction pathways (Crounse, Nielsen, et al., 2013). This correlation with τ_{RO_2} is illustrated in Figure 4.2.

It appears that for bimolecular lifetimes $<<$ 1 s, the SOA yield $< 10\%$. This is congruent with past studies of 2-EE SOA formation in the presence of NO_x and H_2O_2. In low τ_{RO_2} where NO is present, products such as ethoxy-nitrate were observed, as illustrated in Figure 4.3. We were, however, unable to confirm the presence the hydroperoxy nitrate product, similar to past work (Yu et al., 2023). Though it appears some NO-products form, given the relatively low SOA yield, it may be that the nitrate products have a very low yield. Similar to past work, we observe the formation of 2-OH-ethylformate, a C3 product that forms under high-NO conditions (Yu et al., 2023). Colmenar et al. also proposed several fragmentation products in the NO oxidative pathway of 2-EE, such as formaldehyde, glcolaldehyde, and acetaldehyde.

HO_2 pathways led to the formation of an ethoxyethanol ketone product (EE=O) and significant amounts of ethoxyethanol hydroperoxide (EE-OOH) (Figure 4.4). RO_2/RO_2 chemistry can similarly lead to the formation of EE=O. We also observe the

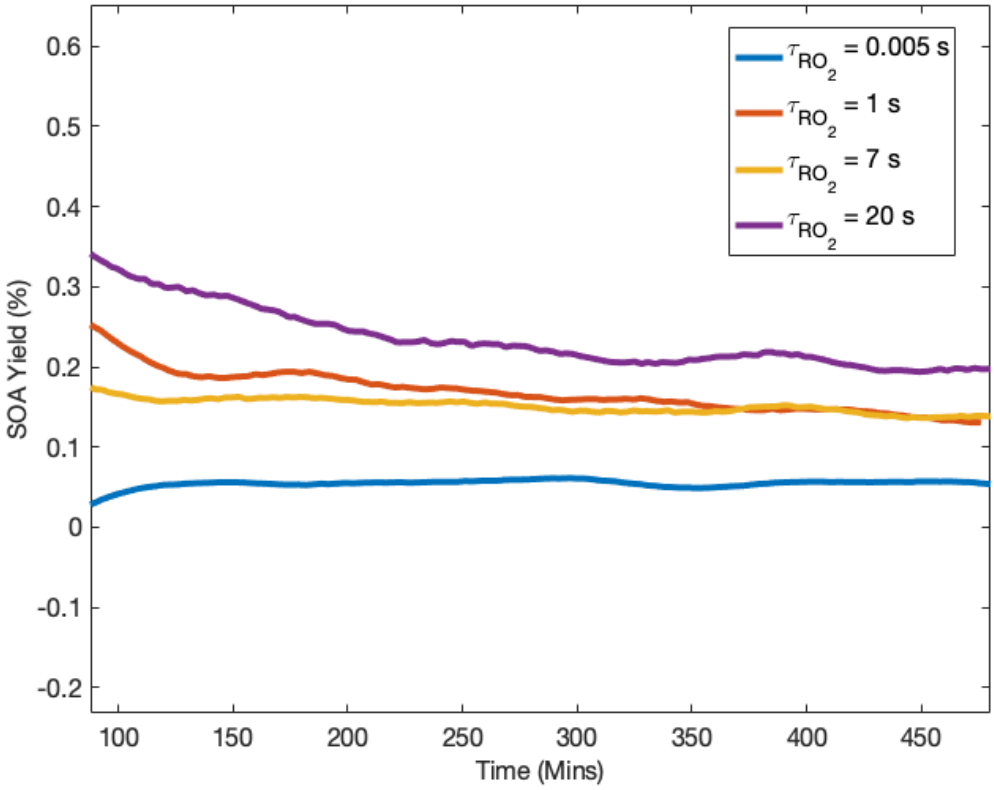

Figure 4.2: SOA yields from ethoxyethanol reactions are correlated with bimolecular lifetimes.

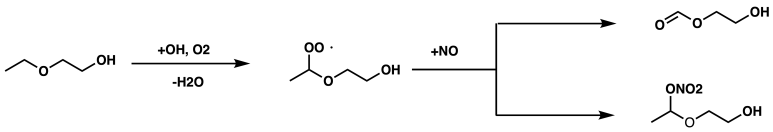

Figure 4.3: Nitrate formation from ethoxethanol photooxidation.

RO_2 product hydroxy-EE (EE-OH). These high O:C ratio photooxidation products illustrate how greater amounts of SOA are likely formed than in high-NO conditions.

If the bimolecular lifetime is sufficient, the peroxy radical intermediate can undergo a 1,5 H-shift to form a peroxy hydroperoxy radical intermediate (OO-EE-OOH). This radical intermediate can then undergo additional HO_2 chemistry. We observe the formation of a hydroperoxy ketone product that likely forms as the result of HO_2 reaction with the OO-EE-OOH intermediate (Figure 4.5). We do not, however, observe the di-hydroperoxy product proposed in past work, though it is not observed explicitly in Yu et al. either (Yu et al., 2023).

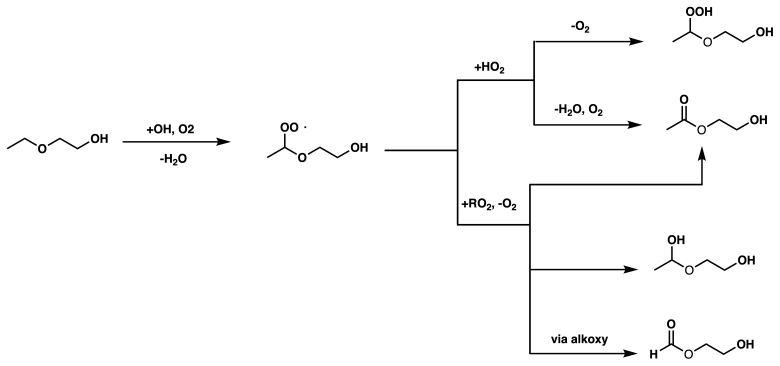

Figure 4.4: HO_2 and RO_2 pathways for ethoxyethanol photooxidation.

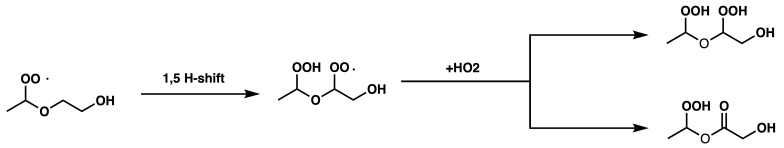

Figure 4.5: HO_2 can react with the hydroperoxy peroxy radical to form additional oxygenated products. Note that we do not observe the di-hydroperoxy product.

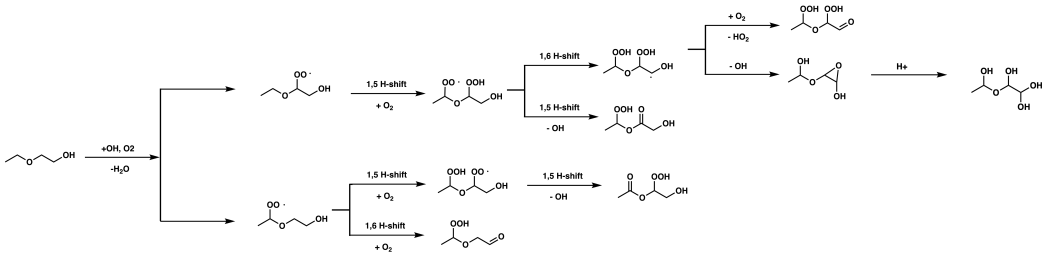

Figure 4.6: Autoxidation chemistry of 2-EE.

When bimolecular lifetimes are $\sim$ 20 s, we see the SOA yield reaches $>$ 20%. In this chemical regime, $>$ 30% of RO_2 formed will undergo an H-shift. We see formation of one such H-shift product, the hydroperoxy ketone (OOH-EE=O) as illustrated in Figure 4.6. We observe very little to no gas-phase formation of the di-hydroperoxy aldehyde (OOH-EE-CHO), the hydroperoxy hydroxy ketone (oxo-EE-ROOH), or epoxide products also illustrated in Figure 4.6. This does not necessarily preclude their existence.

Using EPA OPERA to estimate the physicochemical properties of these compounds of these products, we estimate the saturation mass concentration (C*) for some of the hypothesized products (Environmental Protection Agency (EPA), 2017). Based on the volatility basis set, we can estimate to what degree products may be in the particle or gas phase. Compounds with $C^* < 1 \times 10^{-2}$ $\nu g\,m^{-3}$ always exist in the

particle phase and those with the C* $\approx 10^2$ μg m^{-3} exist significantly in both gas and particle phase (Seinfeld et al., 2016). Therefore, based on Table 4.3, it is reasonable to assume that all or large quantities of these compounds, if present, exist in the particulate phase and thus may not be detectable using the CF_{30}^- CIMS described in the methodology section. The formation of products like oxo-EE-OOH illustrate how the autoxidation pathway can rapidly form highly oxygnated organic molecules; past work calculates that the H-shift rates in the 2-EE system ≤ 0.1 s^{-1} (Yu et al., 2023).

Compound	C* (μg m^{-3})
di-OOH-EE-CHO	5.7×10^2
epoxy-EE-OOH	4.2×10^{-1}

Table 4.3: C* values calculated for selected proposed 2-EE photoxidation products. For hydroperoxy compounds, equivalent hydroxy compounds were used as proxy structures.

Experiment EE2 has a comparable bimolecluar lifetime to that of EE3 but was conducted at higher temperature. The hydrogen shift reaction rates with RO_2 can occur faster at higher temperatures (Praske et al., 2018). We find, however, that the SOA yield rate is lower at ~ 10°C higher temperature: 13%. Despite autoxidation products forming at faster rates, the higher temperatures likely lead to reduced partition into the particle phase. It may be in experiment EE2 that temperature effects out compete kinetics in SOA formation.

4.5 Conclusion

The aerosol formation from 2-EE was investigated under a range of peroxy radical bimolecular lifetimes. The bimolecular lifetimes were varied by changing NO, HO_2, and hν conditions.

The SOA yield of 2-EE varies from 22% to 4.5%. The RO_2 bimolecular lifetime, τ_{RO_2}, appears to be positively correlated to SOA yield. We hypothesize that at larger τ_{RO_2}, more H-shift reactions occur with RO_2 radicals, leading to highly oxygenated products. These oxidation products then efficiently partition to the particle phase. We observe gas-phase products congruent with past work (Yu et al., 2023; Colmenar et al., 2020). Oxidation products include highly oxygenated compounds with O:C ratios greater than unity. At higher temperature, where the autoxidation kinetics should be faster, we find less SOA forms, likely because the oxidation products are more likely to remain in the gas-phase.

In high NO conditions we observe nitrates but we also observe a C3 product. Formation of C3 products and other fragmentation products may contribute to the lower SOA Y in high NO experiments.

Understanding the SOA formation of 2-EE as a model for glycol ethers is important as NO_x regimes continue to evolve in urban centers. This work helps to characterize the effects of VCPs on SOA and to potentially better resolve discrepancies between SOA observations and models.

APPENDIX

4.6 Calculation of Bimolecular Lifetime

Reaction rates of the peroxy radical with NO and HO_2 are presented in this section (Table SI.4.4). $[HO_2]$ was calculated by considering the production and mechanisms of HO_2 (Praske et al., 2018). The production of HO_2 is dominated by the H_2O_2 reaction and the loss of HO_2 is dominated by the $HO_2{}^+HO_2$ self-reaction, such that:

$$P_{H_2O_2} = k_{HO_2{}^+HO_2} \times [HO_2]^2 \tag{4.7}$$

Rearranging Eq.4.7 gives the HO_2 mixing ratio as:

$$[HO_2] = \sqrt{\frac{P_{H_2O_2}}{k_{H_2O_2}}}. \tag{4.8}$$

In Experiments EE1 where [NO] = 0 and [MeOH] = 0, $[HO_2]$ was estimated using a box model which incorporated reactions of ethoxyethanol represented in MCM as well as chemistry discussed in Yu et al. 2023 (Jenkin et al., 1997; Saunders et al., 2003; Yu et al., 2023). The error of the calculated bimolecular lifetime, therefore, is larger for these two experiments.

$k_{RO_2{}^+NO}$ ($cm^3\ molec^{-1} s^{-1}$)	$k_{RO_2{}^+HO_2}$ ($cm^3\ molec^{-1} s^{-1}$)
8.9×10^{-12}	2.2×10^{-11}

Table 4.4: Kinetic rates used to calculate peroxy radical bimolecular lifetime from Jenkin et al., 2003.

Chapter 5

FUTURE WORK

The history of air quality regulation underscores the importance of scientific research in informing the evolving policy landscape. The past several decades have seen remarkable progress in both the scientific understanding and regulatory aspects of air quality and atmospheric chemistry. Still yet, challenges remain.

Despite significant improvements, in many regions of the country, ground-level NO_x, ozone, and particulate matter remain at unhealthy levels. It is clear as the composition of atmospheric VOCs continues to evolve and as NO_x continue to decrease, scientific input into the regulatory process will continue to be key. Continue work on understanding the growing importance of VCP emssions and autoxidation is important both to the growing opus of atmospheric chemistry research and to making well-informed policy decisions.

Chemistry of Other Glycol Ethers

As discussed in Chapter 4, glycol ethers are prevalent in VCPs such as cleaning products, paints, and coatings. Past chamber studies on glycol ethers hypothesized a molecular structural correlation to SOA yield (Li et al., 2018). This hypothesis was that compounds with a structure of $R-(C_nH_{2n}O_m)-OH$ formed more SOA compared to those with a structure of $R-(C_nH_{2n}O_m)-H$ Li et al., 2018. This is because the glycol ethers with a functional OH group form cyclic products that reduce cleavage and thus fragmentation during oxidation Li et al., 2018. These lower volatility cyclic products go on to form high O:C ratio ketones that can partition to the particle phase. By contrast, the glycol ethers without an OH group more readily fragment and therefore have a much lower SOA formation potential. This hypothesis was further tested by using methyl groups in methoxyethoxymethylpropanol to sterically hinder access to the OH functional group and thus decreasing its SOA potential. A full list of glycol ethers used by Li et al. (2018) can be found in Table 5.1.

Li et al. experiments were performed under three conditions: H_2O_2-only, NO-only, and H_2O_2 + OH. HR-ToF-AMS analysis was used to determine bulk chemical properties of the SOA formed by the glycol ethers. Analytes fragmented by the

were further used to infer the functional groups of oxidation products in the particle phase. A SIFT-MS with H_3O^+, NO^+, and $O_2{}^+$ ion sources. The analysis from this instrument confirmed the presence of cyclic compounds in the gas phase.

Future work could re-probe some of the glycol ethers in the Li study or probe similarly structured, proxy compounds. Additional studied could probe a wider range of NO_x levels and peroxy radical bimolecular lifetimes. Not all compounds would necessarily need to be restudied, per se. Instead, studies that look at patterns in molecular structure will be key for predicting SOA potential for larger classes of compounds and chemical structures.

These future studies could see if the OH functional group continues to play an important role at different NO_x and HO_2 levels. Using the GC-CIMS, a specific mechanism could be developed for the proposed cyclization of the glycol ethers. It would be interesting to understand what is required to active the cyclization chemistry—for example, if the position of the OH functional group matters or if number of carbons matter. Though Li proposed OH plays an important role in SOA formation, DEGME, which has a terminal OH group, formed insignificant amount of SOA in low NO conditions. On the other hand, EGDEE, which has no hydroxyl groups, formed a significant amount of SOA.

Initial research on these glycol ethers could use quantum calculation techniques used elsewhere to estimate the kinetics of various H-shifts for different glycol ethers (Murphy et al., 2023; Xu et al., 2020; Yu et al., 2023). This may provide insight into which compounds may be likely to autoxidize and narrow down which compounds may be interesting to study in a laboratory setting.

Other glycol ethers and esters likely also form low vapor pressure, high O:C ratio products via autoxidation under similar atmospherically relevant conditions. While 2-EE demonstrates this chemistry, larger glycol ethers and esters intrinsically have lower vapor pressures (because vapor pressure correlates with molecular weight) and therefore will likely autoxidize to form low volatility products more efficiently, thereby partitioning to the particle-phase more effectively. It is imperative to consider glycol ether and ester autoxidation in future models including CMAQ.

Compound	Structure	SOA Potential
Diethylene glycol butyl ether (DEGBE)	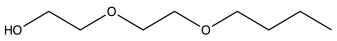	Largest $M_o > 15\mu g\ m^{-1}$
Di(propylene glycol) butyl ether (DPGBE)	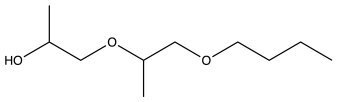	$M_o > 15\mu g\ m^{-1}$
2,2-Diethoxy-1-propanol (33D1P)	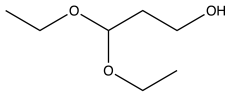	$M_o > 15\mu g\ m^{-1}$
1,3-Diethoxy-2-propanol (13D2P)	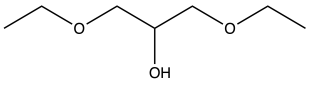	$M_o > 15\mu g\ m^{-1}$
Diethylene glycol ethyl ether (DEGEE)	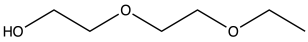	$M_0 > 15\mu g\ m^{-1}$
Ethylene glycol diethyl ether (EGDEE)	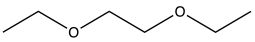	$M_0 \approx 3 - 5\mu g m^{-1}$
Diethylene glycol methyl ether (DEGME)	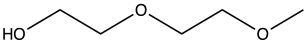	under NO_x-only conditions
1-(2-Methoxyethanoxy)-2-methyl-2-propanol (12M2MP)	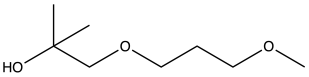	$M_o < 3\mu g\ m^{-3}$
Diethylene glycol dimethyl ether (DEGDME)	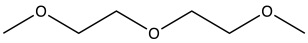	$M_o < 3\mu g\ m^{-3}$
Dimethoxyethane	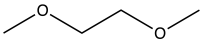	$M_o < 3\mu g\ m^{-3}$

Table 5.1: Glycol ethers studied in Li and Cocker 2018, listed from top to bottom in order of SOA potential.

Box Model

One of the most cited box models during my time in graduate school is the work done by McDonald et al. 2018. Since its publication, our lab and others have updated information on the chemistry of and SOA yields from a variety of VOCs considered. Pennington et al. integrated much of this work into an update of the Environmental Protection Agency's (EPA's) Community Mulitscale Air Quality (CMAQ) model so that SOA formed from VPC emissions could be better represented (Pennington et al., 2021). CMAQ represents ambient air quality while McDonald et al. also attempted to model indoor air. An interesting project could revisit the McDonald box model of indoor air quality using similar assumptions about air exchange and OH exposure but updating the SOA potential of recently studied VCP solvents and

particularly those studied at a range of OH exposure and NO conditions as discussed in earlier chapters (see also Appendix B).

Contribution to CRACMM

An update to the CMAQ model discussed in the previous subsection aims to update the chemical speciation and reactive pathways of ROCs vis-a-vis a new add-in called the Community Regional Atmospheric Chemistry Multiphase Model (CRACMM) (Environmental Protection Agency (EPA), n.d.). The "community" aspect refers to an open-source framework approach where scientists can provide technical input to the model. CRACMM will specify chemistry for gas-phase and particle-phase pathways and is meant to include a more comprehensive set of precursor species and chemical mechanisms. EPA indicates that from 2023 - 2025, CRACMM will continue "developing, testing, evaluating, and documenting" updates and results with input from the broader scientific community (Environmental Protection Agency (EPA), n.d.). The goal is to ultimately have CRACMM used as the default mechanism in CMAQ by 2025 (Environmental Protection Agency (EPA), n.d.).

This call to the atmospheric chemistry community provides an opportunity for a future researcher to incorporate insights from our recent laboratory work into CRACMM. While past work aimed to develop add-ins for VCPs to be represented in CMAQ, CRACMM allows for more explicit chemical representation (Pennington et al., 2021; Seltzer et al., 2021). A future project could focus representing new glycol ethers and ethers chemistry to CRACMM. This would include developing explicit emissions inventories for recently studied VPCs in our labs and developing an add-in to represent their autoxidation chemistry as well as HO_2 and NO chemistry for CRACMM. A comparison can then determine the effects of including these additional compounds and their chemistry by running CMAQ with the updates to CRACMM and comparing the results with and without the glycol ethers and esters and with observations.

In general, autoxidation will be incorporated into CRACMM v1.0, however only for larger alkanes, aromatics, sesquiterpenes, and monoterpenes (Environmental Protection Agency (EPA), n.d.; Pye et al., 2023). So there is also the opportunity to include an relevant autoxidation chemistry outside of these general categories.

This work would be particularly suitable for a future research interested in participating in the NSF-funded INTERN program for researching conducted at EPA facilities or an ORISE internship.

BIBLIOGRAPHY

(EPA), Environmental Protection Agency (2016). *Glycol Ethers*. URL: https://www.epa.gov/sites/default/files/2016-09/documents/glycol-ethers.pdf.

Aschmann, Sara M. and Roger Atkinson (1998). "Kinetics of the gas-phase reactions of the oh radical with selected glycol ethers, glycols, and alcohols". en. In: *International Journal of Chemical Kinetics* 30.8, pp. 533–540. ISSN: 0538-8066, 1097-4601. DOI: 10.1002/(SICI)1097-4601(1998)30:8<533::AID-KIN2>3.0.CO;2-T. URL: https://onlinelibrary.wiley.com/doi/10.1002/(SICI)1097-4601(1998)30:8%3C533::AID-KIN2%3E3.0.CO;2-T (visited on 03/18/2024).

Chan, Man Nin, Jason D. Surratt, Magda Claeys, Eric S. Edgerton, Roger L. Tanner, Stephanie L. Shaw, Mei Zheng, Eladio M. Knipping, Nathan C. Eddingsaas, Paul O. Wennberg, and John H. Seinfeld (June 2010). "Characterization and quantification of isoprene-derived epoxydiols in ambient aerosol in the southeastern United States". en. In: *Environmental Science & Technology* 44.12, pp. 4590–4596. ISSN: 0013-936X, 1520-5851. DOI: 10.1021/es100596b. URL: https://pubs.acs.org/doi/10.1021/es100596b (visited on 10/24/2023).

Charan, Sophia M., Reina S. Buenconsejo, and John H. Seinfeld (Nov. 2020). "Secondary organic aerosol yields from the oxidation of benzyl alcohol". en. In: *Atmospheric Chemistry and Physics* 20.21, pp. 13167–13190. ISSN: 1680-7324. DOI: 10.5194/acp-20-13167-2020. URL: https://acp.copernicus.org/articles/20/13167/2020/ (visited on 10/26/2021).

Charan, Sophia M., Yuanlong Huang, and John H. Seinfeld (Dec. 2019). "Computational simulation of secondary organic aerosol formation in laboratory chambers". en. In: *Chemical Reviews* 119.23, pp. 11912–11944. ISSN: 0009-2665, 1520-6890. DOI: 10.1021/acs.chemrev.9b00358. URL: https://pubs.acs.org/doi/abs/10.1021/acs.chemrev.9b00358 (visited on 11/30/2020).

Charan, Sophia M., Weimeng Kong, Richard C. Flagan, and John H. Seinfeld (Aug. 2018). "Effect of particle charge on aerosol dynamics in Teflon environmental chambers". en. In: *Aerosol Science and Technology* 52.8, pp. 854–871. ISSN: 0278-6826, 1521-7388. DOI: 10.1080/02786826.2018.1474167. URL: https://www.tandfonline.com/doi/full/10.1080/02786826.2018.1474167 (visited on 11/30/2020).

Colmenar, Inmaculada, Sagrario Salgado, Pilar Martín, Inmaculada Aranda, Araceli Tapia, and Beatriz Cabañas (Mar. 2020). "Tropospheric reactivity of 2-ethoxyethanol with OH and NO3 radicals and Cl atoms. Kinetic and mechanistic study". en. In: *Atmospheric Environment* 224, p. 117367. ISSN: 13522310. DOI: 10.1016/j.atmosenv.2020.117367. URL: https://linkinghub.elsevier.com/retrieve/pii/S1352231020301060 (visited on 03/19/2024).

Crounse, John D., Hasse C. Knap, Kristian B. Ørnsø, Solvejg Jørgensen, Fabien Paulot, Henrik G. Kjaergaard, and Paul O. Wennberg (June 2012). "Atmospheric fate of methacrolein. 1. peroxy radical isomerization following addition of OH and O2". en. In: *The Journal of Physical Chemistry A* 116.24, pp. 5756–5762. ISSN: 1089-5639, 1520-5215. DOI: 10.1021/jp211560u. URL: https://pubs.acs.org/doi/10.1021/jp211560u (visited on 09/06/2023).

Crounse, John D., Karena A. McKinney, Alan J. Kwan, and Paul O. Wennberg (Oct. 2006). "Measurement of gas-phase hydroperoxides by chemical ionization mass spectrometry". en. In: *Analytical Chemistry* 78.19, pp. 6726–6732. ISSN: 0003-2700, 1520-6882. DOI: 10.1021/ac0604235. URL: https://pubs.acs.org/doi/10.1021/ac0604235 (visited on 03/15/2024).

Crounse, John D., Lasse B. Nielsen, Solvejg Jørgensen, Henrik G. Kjaergaard, and Paul O. Wennberg (Oct. 2013). "Autoxidation of organic compounds in the atmosphere". en. In: *The Journal of Physical Chemistry Letters* 4.20, pp. 3513–3520. ISSN: 1948-7185, 1948-7185. DOI: 10.1021/jz4019207. URL: https://pubs.acs.org/doi/10.1021/jz4019207 (visited on 10/28/2021).

Environmental Protection Agency (EPA) (Jan. 2017). *CTS: Chemical Transformation Simulator*. URL: https://qed.epa.gov/cts/chemspec/.

– (n.d.). *Community regional atmospheric chemistry multiphase mechanism (CRACMM) for improving air quality modeling*.

Li, Lijie and David R. Cocker (May 2018). "Molecular structure impacts on secondary organic aerosol formation from glycol ethers". en. In: *Atmospheric Environment* 180, pp. 206–215. ISSN: 13522310. DOI: 10.1016/j.atmosenv.2017.12.025. URL: https://linkinghub.elsevier.com/retrieve/pii/S1352231017308610 (visited on 01/26/2019).

Lopes, M., L. Serrano, I. Ribeiro, P. Cascão, N. Pires, S. Rafael, L. Tarelho, A. Monteiro, T. Nunes, M. Evtyugina, O.J. Nielsen, M. Gameiro Da Silva, A.I. Miranda, and C. Borrego (Feb. 2014). "Emissions characterization from EURO 5 diesel/biodiesel passenger car operating under the new European driving cycle". en. In: *Atmospheric Environment* 84, pp. 339–348. ISSN: 13522310. DOI: 10.1016/j.atmosenv.2013.11.071. URL: https://linkinghub.elsevier.com/retrieve/pii/S1352231013009217 (visited on 03/18/2024).

Murphy, Sara E., John D. Crounse, Kristian H. Møller, Samir P. Rezgui, Nicholas J. Hafeman, James Park, Henrik G. Kjaergaard, Brian M. Stoltz, and Paul O. Wennberg (2023). "Accretion product formation in the self-reaction of ethene-derived hydroxy peroxy radicals". en. In: *Environmental Science: Atmospheres* 3.5, pp. 882–893. ISSN: 2634-3606. DOI: 10.1039/D3EA00020F. URL: http://xlink.rsc.org/?DOI=D3EA00020F (visited on 09/06/2023).

Nguyen, T. B., M. M. Coggon, K. H. Bates, X. Zhang, R. H. Schwantes, K. A. Schilling, C. L. Loza, R. C. Flagan, P. O. Wennberg, and J. H. Seinfeld (Apr. 2014). "Organic aerosol formation from the reactive uptake of isoprene epoxydiols

(IEPOX) onto non-acidified inorganic seeds". en. In: *Atmospheric Chemistry and Physics* 14.7, pp. 3497–3510. ISSN: 1680-7324. DOI: 10.5194/acp-14-3497-2014. URL: https://www.atmos-chem-phys.net/14/3497/2014/ (visited on 01/09/2019).

Parker, H. A., S. Hasheminassab, J. D. Crounse, C. M. Roehl, and P. O. Wennberg (Dec. 2020). "Impacts of Traffic Reductions Associated With COVID-19 on Southern California Air Quality". en. In: *Geophysical Research Letters* 47.23. ISSN: 0094-8276, 1944-8007. DOI: 10.1029/2020GL090164. URL: https://onlinelibrary.wiley.com/doi/10.1029/2020GL090164 (visited on 05/22/2023).

Pennington, Elyse A., Karl M. Seltzer, Benjamin N. Murphy, Momei Qin, John H. Seinfeld, and Havala O. T. Pye (Dec. 2021). "Modeling secondary organic aerosol formation from volatile chemical products". en. In: *Atmospheric Chemistry and Physics* 21.24, pp. 18247–18261. ISSN: 1680-7324. DOI: 10.5194/acp-21-18247-2021. URL: https://acp.copernicus.org/articles/21/18247/2021/ (visited on 05/19/2022).

Praske, Eric, Rasmus V. Otkjær, John D. Crounse, J. Caleb Hethcox, Brian M. Stoltz, Henrik G. Kjaergaard, and Paul O. Wennberg (Jan. 2018). "Atmospheric autoxidation is increasingly important in urban and suburban North America". en. In: *Proceedings of the National Academy of Sciences* 115.1, pp. 64–69. ISSN: 0027-8424, 1091-6490. DOI: 10.1073/pnas.1715540115. URL: http://www.pnas.org/lookup/doi/10.1073/pnas.1715540115 (visited on 08/13/2018).

Pye, Havala O. T., Bryan K. Place, Benjamin N. Murphy, Karl M. Seltzer, Emma L. D'Ambro, Christine Allen, Ivan R. Piletic, Sara Farrell, Rebecca H. Schwantes, Matthew M. Coggon, Emily Saunders, Lu Xu, Golam Sarwar, William T. Hutzell, Kristen M. Foley, George Pouliot, Jesse Bash, and William R. Stockwell (May 2023). "Linking gas, particulate, and toxic endpoints to air emissions in the Community Regional Atmospheric Chemistry Multiphase Mechanism (CRACMM)". en. In: *Atmospheric Chemistry and Physics* 23.9, pp. 5043–5099. ISSN: 1680-7324. DOI: 10.5194/acp-23-5043-2023. URL: https://acp.copernicus.org/articles/23/5043/2023/ (visited on 08/22/2023).

Seinfeld, John H. and Spyros N. Pandis (2016). *Atmospheric chemistry and physics: From air pollution to climate change*. en. Third edition. Hoboken, New Jersey: John Wiley & Sons. ISBN: 978-1-119-22116-6 978-1-119-22117-3.

Seltzer, Karl M., Elyse Pennington, Venkatesh Rao, Benjamin N. Murphy, Madeleine Strum, Kristin K. Isaacs, and Havala O. T. Pye (Mar. 2021). "Reactive organic carbon emissions from volatile chemical products". en. In: *Atmospheric Chemistry and Physics* 21.6, pp. 5079–5100. ISSN: 1680-7324. DOI: 10.5194/acp-21-5079-2021. URL: https://acp.copernicus.org/articles/21/5079/2021/ (visited on 11/29/2022).

Simon, Heather, Adam Reff, Benjamin Wells, Jia Xing, and Neil Frank (Jan. 2015). "Ozone Trends Across the United States over a Period of Decreasing NOx and VOC Emissions". en. In: *Environmental Science & Technology* 49.1, pp. 186–195. ISSN: 0013-936X, 1520-5851. DOI: 10.1021/es504514z. URL: https://pubs.acs.org/doi/10.1021/es504514z (visited on 09/06/2023).

Singer, B. C., H. Destaillats, A. T. Hodgson, and W. W. Nazaroff (June 2006). "Cleaning products and air fresheners: Emissions and resulting concentrations of glycol ethers and terpenoids". en. In: *Indoor Air* 16.3, pp. 179–191. ISSN: 0905-6947, 1600-0668. DOI: 10.1111/j.1600-0668.2005.00414.x. URL: http://doi.wiley.com/10.1111/j.1600-0668.2005.00414.x (visited on 02/05/2021).

Stemmler, Konrad, David J. Kinnison, and J. Alistair Kerr (Jan. 1996). "Room Temperature Rate Coefficients for the Reactions of OH Radicals with Some Monoethylene Glycol Monoalkyl Ethers". en. In: *The Journal of Physical Chemistry* 100.6, pp. 2114–2116. ISSN: 0022-3654, 1541-5740. DOI: 10.1021/jp9520355. URL: https://pubs.acs.org/doi/10.1021/jp9520355 (visited on 03/18/2024).

Stemmler, Konrad, Wolfgang Mengon, David J. Kinnison, and J. Alistair Kerr (Apr. 1997). "OH Radical-Initiated Oxidation of 2-Butoxyethanol under Laboratory Conditions Related to the Troposphere: Product Studies and Proposed Mechanism". en. In: *Environmental Science & Technology* 31.5, pp. 1496–1504. ISSN: 0013-936X, 1520-5851. DOI: 10.1021/es9607547. URL: https://pubs.acs.org/doi/10.1021/es9607547 (visited on 03/18/2024).

Surratt, Jason D., Arthur W. H. Chan, Nathan C. Eddingsaas, ManNin Chan, Christine L. Loza, Alan J. Kwan, Scott P. Hersey, Richard C. Flagan, Paul O. Wennberg, and John H. Seinfeld (Apr. 2010). "Reactive intermediates revealed in secondary organic aerosol formation from isoprene". en. In: *Proceedings of the National Academy of Sciences* 107.15, pp. 6640–6645. ISSN: 0027-8424, 1091-6490. DOI: 10.1073/pnas.0911114107. URL: https://pnas.org/doi/full/10.1073/pnas.0911114107 (visited on 09/06/2023).

World Health Organization (2024). *Air Pollution*. URL: https://www.who.int/health-topics/air-pollution#tab=tab_2.

Xu, Lu, Kristian H. Møller, John D. Crounse, Henrik G. Kjaergaard, and Paul O. Wennberg (Nov. 2020). "New Insights into the Radical Chemistry and Product Distribution in the OH-Initiated Oxidation of Benzene". en. In: *Environmental Science & Technology* 54.21, pp. 13467–13477. ISSN: 0013-936X, 1520-5851. DOI: 10.1021/acs.est.0c04780. URL: https://pubs.acs.org/doi/10.1021/acs.est.0c04780 (visited on 01/31/2022).

Yu, Hongmin, Kristian H. Møller, Reina S. Buenconsejo, John D. Crounse, Henrik G. Kjaergaard, and Paul O. Wennberg (Nov. 2023). "Atmospheric photo-oxidation of 2-ethoxyethanol: autoxidation chemistry of glycol ethers". en. In: *The Journal of Physical Chemistry A*, acs.jpca.3c04456. ISSN: 1089-5639, 1520-5215. DOI:

10.1021/acs.jpca.3c04456. URL: https://pubs.acs.org/doi/10.1021/acs.jpca.3c04456 (visited on 11/15/2023).